TÜBİTAK

Turkish Journal of Earth Sciences

http://journals.tubitak.gov.tr/earth/

Research Article

Turkish J Earth Sci
(2023) 32: 447-469

doi:10.55730/1300-0985.1855

# Neotectonic and topographic evolution of the Bitlis-Zagros Fold-Thrust Belt, SE Turkey

**Halil ZORER[1,*], Yahya ÖZTÜRK[2], Azad SAĞLAM SELÇUK[3,4,*]**
[1]Department of Geography, Van Yüzüncü Yıl University, Van, Turkey
[2]Institute of Social Sciences, Van Yüzüncü Yıl University, Van, Turkey
[3]Department of Geological Engineering, Van Yüzüncü Yıl University, Van, Turkey
[4]Institute of Natural and Applied Sciences, Van Yüzüncü Yıl University, Van, Turkey

**Received:** 06.10.2022 • **Accepted/Published Online:** 06.03.2023 • **Final Version:** 29.05.2023

**Abstract:** The Bitlis-Zagros Fold-Thrust Belt is one of the world's largest deformation zones, extending from the Eastern Mediterranean in southern Turkey to in the south of Iran. This deformation zone is partitioned between different structures; however, little is known about the relative activities of these different structures and their effects on topography. An area located in the northern part of Bitlis-Zagros Fold-Thrust Belt, just south of the Eastern Anatolian Plateau was studied in detail to analyze the effect of active tectonism on topographic development. The effects of active deformation structures such as Hakkâri and Şirvan Fault Segments on the topographic evolution of Kato Folds and Sinebel Valley were investigated to understand the fold and thrust fault activity. Geomorphic indices were used, such as *HC, HI, SR, Ksn* together with rose analysis based on bedding measurements. Investigation of folding in the region indicates the effective stress regime in the precollision zone was in NW-SE compression direction. The deformation structures, effective in the postcollision zone developed due to N-S directional compression, and are shown here to have different effects on topography of the region. This study has shown the relative uplift rate is highest in the areas where Hakkâri and Şirvan Segments are pure thrust faults (0.4 mm year$^{-1}$), and lower in the transfer zone (0.2 to 0.4 mm year$^{-1}$) between the segments. As a result of this study, it is concluded that the main deformation structures controlling the topography in the region are not only thrust faults, but also structures that develop in the area of transfer zone.

**Key words:** Bitlis-Zagros Fold-Thrust Belt, geomorphic index, relative uplift rate, topographic evolution, neotectonic activities

## 1. Introduction

The Bitlis-Zagros Fold-Thrust Belt (BZFTB) formed as a result of the collision between the Eurasian and the Arabian Plates and closing of the Neotethys Ocean (Dewey et al., 1986; Şengör, 2005). The BZFTB is part of the Alpine-Himalayan orogenic belt, which extends in the E-W direction starting from the eastern Mediterranean and extending eastwards about 2000 km (Dewey et al., 1973; Dercourt et al., 1986; Stampfli and Borel, 2002; Mouthereau et al., 2012) (Figure 1A).

The BZFTB at the eastern end of the Mediterranean extends eastwards approximately 650 km with a convex curve towards the north and ends at the northeastern Zagros Şemdinli-Yüksekova Fault Zone (Figures 1A and 1B). This region comprises the Euphrates and Tigris River catchment, and the topographic structures on the East Anatolian High Plateau reveal the structural evolution of this region.

The Euphrates and the Tigris River catchment cover an area of 800,000 km$^2$ between the Nile River basin to the west and the Indus River to the east, forming the most important drainage basin in the region (Nicoll, 2010). Rivers in this catchment are not only a vital source of life for the region, but they also reveal the tectonic events of the region by fluvial erosion-deposition processes (Doğan, 2005). Understanding the evolution of this region is of crucial importance, considering it also affects the connection between the Indian-Pacific Ocean and the Mediterranean and Tethys Oceans (Harzhauser et al., 2007; Reuter et al., 2009; Mouthereau et al., 2012).

The BZFTB is subdivided into four NW-trending tectonic zones from northeast to southwest and major faults form the boundaries of each tectonic zone (Jassim and Goff, 2006). The NW-SE trending Zagros Orogen Belt is divided into subtectonic units. From northeast to southwest; the Urumieh-Dokhtar Magmatic Arc, the

* Correspondence: azadsaglam@gmail.com

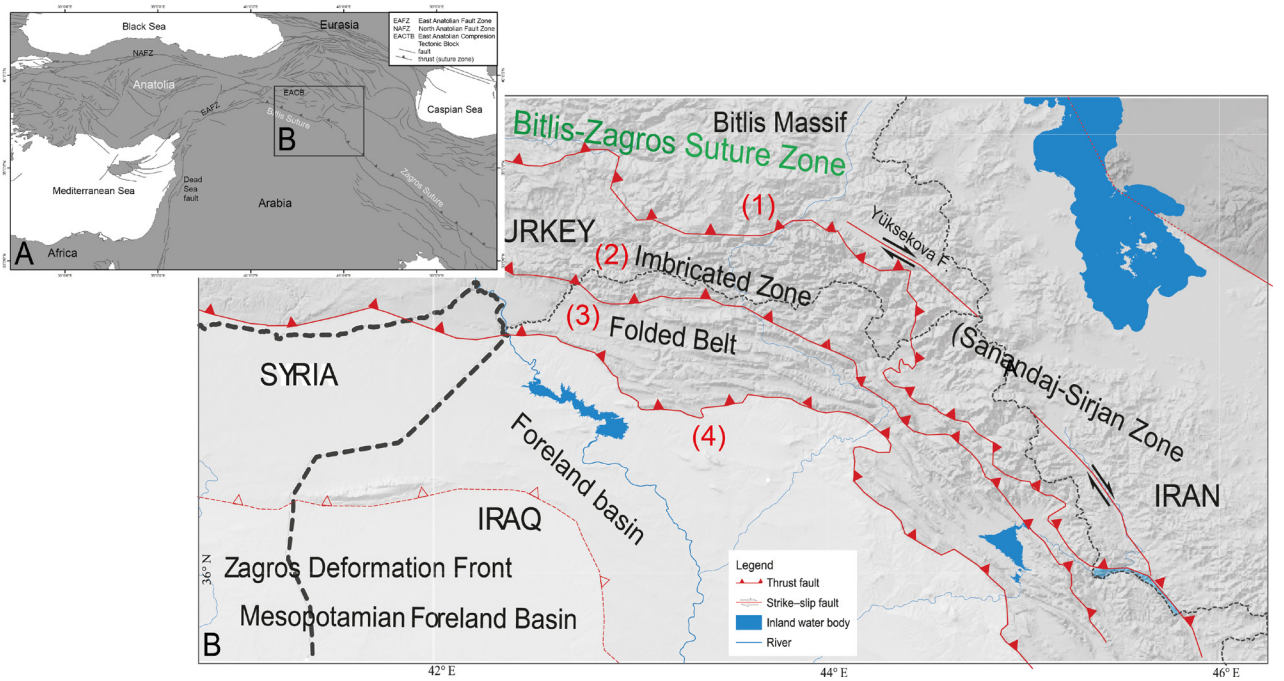


**Figure 1.** A) Tectonic settings of the Eastern Mediterranean and the Middle East. The faults were compiled from various sources (Philip et al., 2001; Hessami et al., 2003; Karakhanian et al., 2004; Emre et al., 2013), B) Tectonic subdivision of the northwestern segment of the BZFTB with the study area highlighted by the blue square (modified after Berberian, 1995; Emre et al., 2013; Zebari and Burberry, 2015; Koshnaw et al., 2017).

metamorphic and magmatic Sanandaj-Sirjan Zone, the Imbricate Zone (High Zagros Thrust Belt), the Simply Folded Belt and the Mesopotamian-Persian Gulf foreland basin (Vegens et al., 2011). These structural belts parallel to each other are bounded by major faults. For example, the Main Zagros Fault (MZF) between the Sanandaj-Sirjan Zone and the Imbricate Zone, the High Zagros Fault between the Imbricate Zone and the Folded Belt, and the Mountain Front Flexure between the Folded Belt and the Mesopotamian-Persian Gulf foreland basin (Vegens et al., 2011) (Figure 1B).

There is ongoing debate about the uplift rate during the last 5–10 Ma (Molinaro et al., 2005a; Allen et al., 2011; Agard et al., 2011; Mouthereau et al., 2012). One of the hypotheses for the internal deformation of the Turkish-Iranian Plateu asserted that there was a reorganization of deformation after the initial collision started 5 ± 2 Ma and the deformation rate of many structures reflect this change (Copley and Jackson, 2006). Contrarily, morphometric studies describe the spatial distribution of significant uplift within the west of Turkish-Iranian Plateau and signify the uplift rate is larger than the horizontal slip rate (Sançar, 2021).

The formation of topographic structures is concerned with the power, mechanism, speed, timing, and duration of the processes that constitute (Allmendinger et al., 1997; Willett, 1999; Stolar et al., 2007; Whipple, 2009; Seyitoğlu et al., 2019, Doski and McClay, 2022). The main factor that promotes to topographic evolution is the ongoing convergence in the active orogens (Bishop, 2007; Burbank and Anderson, 2012; Whittaker, 2012). In recent years, quantitative analysis of the landscape performed thanks to digital elevation models (high-resolution-DEMs) and GIS (geographic information system) software (Bishop, 2007; Tarolli, 2014; Zebari et al., 2019).

Tectonic geomorphology studies are widely applied and effective in investigating the relative tectonic activity of distinctive field, developing in the contractional environment (Ramsey et al., 2008). Such studies have been used to contrast and understand the evolution of folds along the Bitlis Zagros Fold-Thrust Zone (Zebari et al., 2019; Doski and McClay, 2022). It has been observed that the reason for the lateral and vertical folds to reach greater dimensions especially in high folded regions is the progress of folds towards abandoned river channels due to the change of the tectonic regime (Bretis et al., 2011). Zebari et al. (2019) stated that uplift is independent within different segments and that method of estimating relative age difference can be applied to many anticlines in the region to create a model of the temporal evolution of this belt. However, only the effects of thrust faults and compression in the thrust belt on morphology have been

investigated up to now. **Şengör** et al. (1985) stated that in the overall deformational pattern of the East Anatolian contractional province, extensional structures (normal fault, dextral-slip fault etc.) developed in the overstep of the faults in the thrust belt. There is no study on the effect of these extensional structures in the morphological evolution of the region and their relationship between thrust faults.

Thus, the purpose of this study is to reveal the effect of the **Şirvan** and Hakkâri Fault Segments of the BZFTB between Pervari and Beytüşebap (East Anatolia) on the topographic evolution of the region through field studies and quantitative analysis of landscape indices (hypsometric curve, hypsometric integral, surface roughness, and normalized channel steepness index).

In addition, the characteristics of the deformation and erosion occurring in the transfer zone between the steps of segments are not known clearly. One of the main objectives of this study is to reveal the effect of these transfer zones on topography.

## 2. Geological and geomorphological background

The formation of the BZFTB started with the convergence of the Arabian and Eurasian Plates during the late Miocene (Şengör, 1979; Şengör and Yılmaz, 1981; Berberian, 1995), which is a complex ocean-continent; continent-continent collision zone (Şengör, 1979; Şengör and Yılmaz, 1981; Hempton, 1984, 1985; Yiğitbaş and Yılmaz, 1996) (Figures 1A and B). Previous research suggests that there were multiple orogenic events during the Late Cretaceous to Oligocene (Ketin, 1966), with the first thrusting occurring during the Late Cretaceous (Hall, 1976). The mapping of exploration and drilling studies performed by De Righi and Cortesini (1964) defined an upper Cretaceous ophiolitic melange at the Tertiary Arabian Plate. Dewey et al. (1973) suggested that the Bitlis-Zagros Suture Zone started to form as a converging border between the Arabian and Eurasian Plates during the late Miocene. However, the tectonic features and the competency of different sequences are mainly reflected on the topography and geomorphology of the BZFTB (Doski and McClay, 2022). It has been suggested that the BZFTB formed during the fourth stage of the Wilson cycle (Wilson, 1966) and retains features from the Neotetys Ocean basin (Şengör and Yılmaz, 1981).

The length of BZFTB within the borders of Turkey (Kahramanmaraş-Hakkâri) exceeds 650 km (Duman et al., 2017). The faults in the eastern part of the BZFTB in Turkey, where the zone expands over a wide area, were named as the Hakkâri and Şirvan Segments by Duman et al. (2017) (Figures 2 and 3). The Şirvan Segment starts in the northeast of central Siirt and extends for 60 km

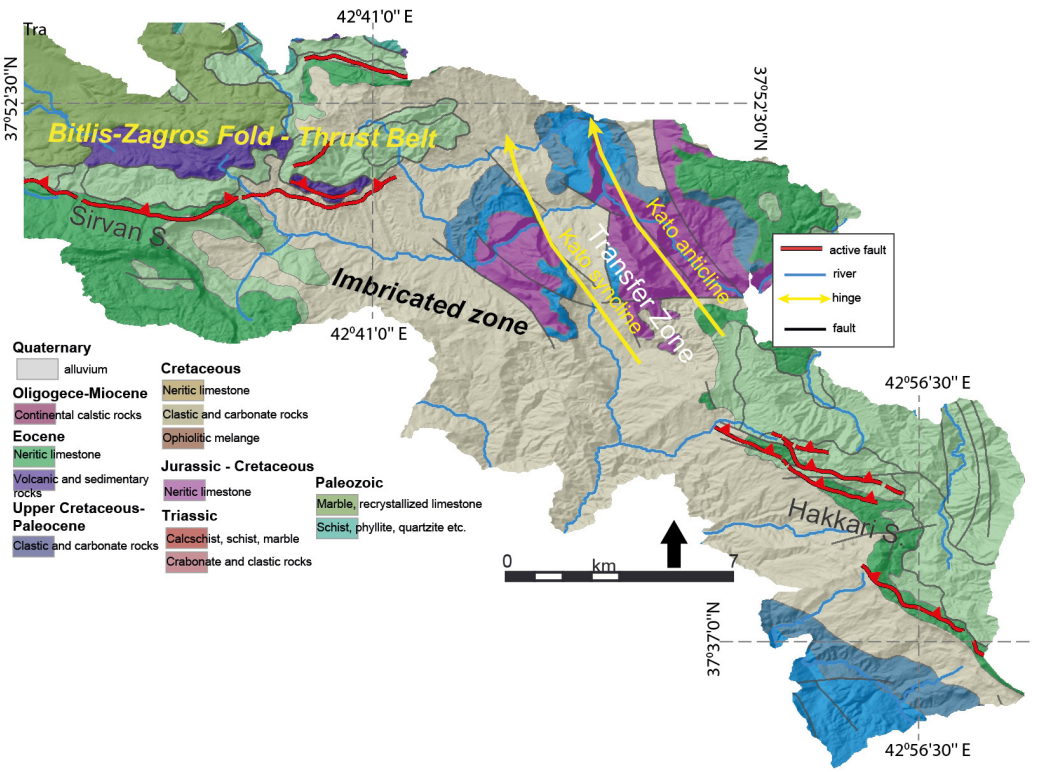


**Figure 2.** The geology of the BZFTB in the south of eastern Anatolia (geology was modified from Sissakian (1997); Csontos et al. (2012) and faults were modified from Emre et al. (2013)).

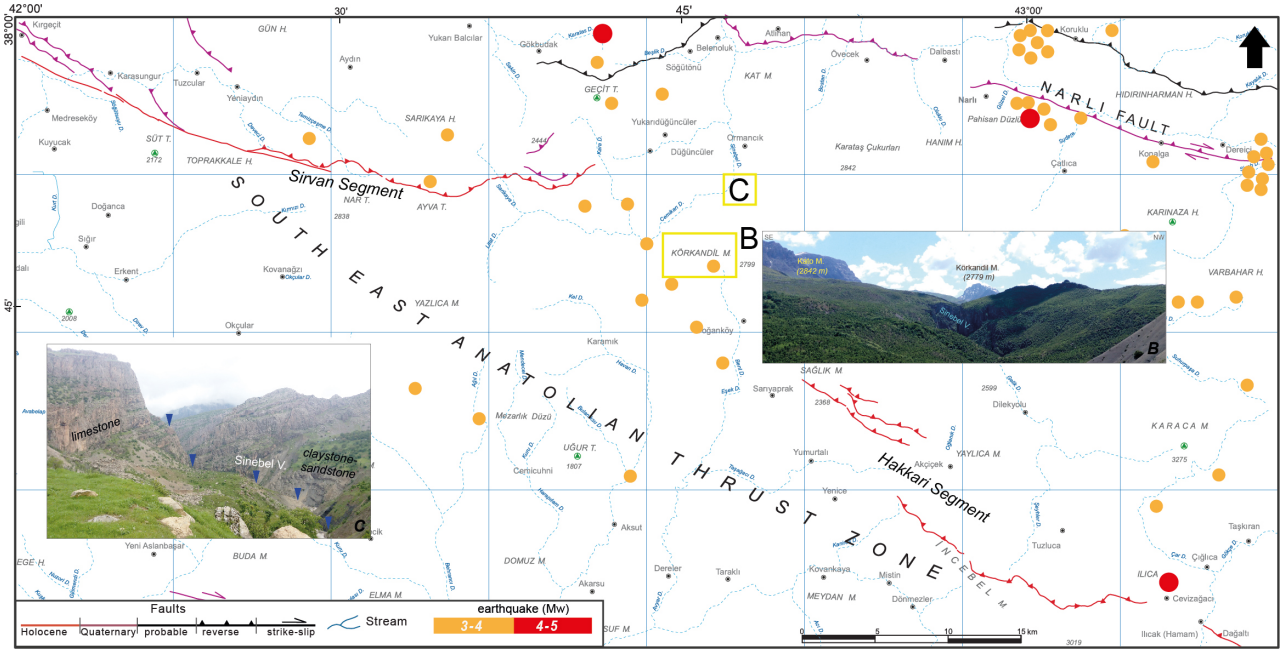


**Figure 3.** A) The topographic and tectonic map of the study area and its surroundings (Cizre NJ 38-9, Emre et al., 2013), B) different geomorphological structures, C) Sinebel Valley and step levels.

towards the east in the direction of N70°-85°W. It is seen that the Şirvan Fault has a right lateral component in some areas along its length. The Hakkâri Segment extends for 19 km with a direction of N85°W and consists of faults developed in a braided pattern in the region.

The other main deformation structures in the BZFTB is folds. It is important to determine the directions of the fold axes, which help to identify the topographic evolution of the region. The main directions of the folds along the suture zone vary the majority of the folds that remain on the borders of Turkey trend N-S or N10-20°W and dip towards the north (Figure 4); however, these folds trends N60-70°W in the Iraq region (Zebari et al., 2019).

The Arabian and Eurasian Plate collision along the BZFTB during the late-mid Miocene led to the uplift of mountains in the suture zone and the transformation from a shallow marine environment to a basin complex (Şengör and Yılmaz, 1981; Duman et al., 2017) (Figure 1A). The merging of Anatolia and Arabia along the BZFTB and the resulting tension in the N-S direction is among the main reasons for the Arabian Plate not being able to move north until the early Pliocene (Hempton, 1987; Robertson et al., 1991; Yılmaz, 1993). The crust of East Anatolia started thickening during the late-mid Miocene to early Pliocene, forming the East Anatolian High Plateau with an elevation of 2000 m (Şengör and Kidd, 1979). According to the paleomagnetic data Arabian Plate is moving northward since the late Cretaceous approximately in the same orientation as in today (Bakkal et al., 2019).

Many deformation structures are present in this region, such as E-W trending thrust faults, folds, and pull-apart basins which formed in response to the change in the tectonic regime from NW-SE to N-S directed compression (Şengör et al., 1985; Kelling et al., 1987). However, during the early Pliocene, the compressional tectonic regime in Eastern Anatolia assumed a right-lateral component (Koçyiğit et al., 2001). Topographic features in the region appear to have been caused by not only approximately E-W directional thrusts and folds, but also approximately N-S oriented normal faults.

The movement of the Anatolian Plate towards the west along the North Anatolian and East Anatolian faults during the early Pliocene allowed the Arabian Plate to move northwards at a higher speed (Oral et al., 1995; Reilinger et al., 1997; Barka and Reilinger, 1997). According to recent GPS-based solid-block models, the Arabian Plate has moved towards the NW at 18 mm year$^{-1}$ relative to the Eurasian Plate (McClusky et al., 2000). It is estimated that compression changes between 10% and 32% in the four different tectonic zones along the BZFTB (Blanc et al., 2003; McQuarrie, 2004; Molinaro et al., 2005b; Mouthereau et al., 2007; Vergés et al., 2011; Zebari et al., 2019). Although, there are some studies addressing the horizontal and vertical component rates of the compression in different regions of the BZFTB (McClusky et al., 2003; Vernant et al., 2004; Reilinger et al., 2006; Hessami et al., 2006; Zebari et al., 2019), the number of studies in Eastern Anatolia is limited.

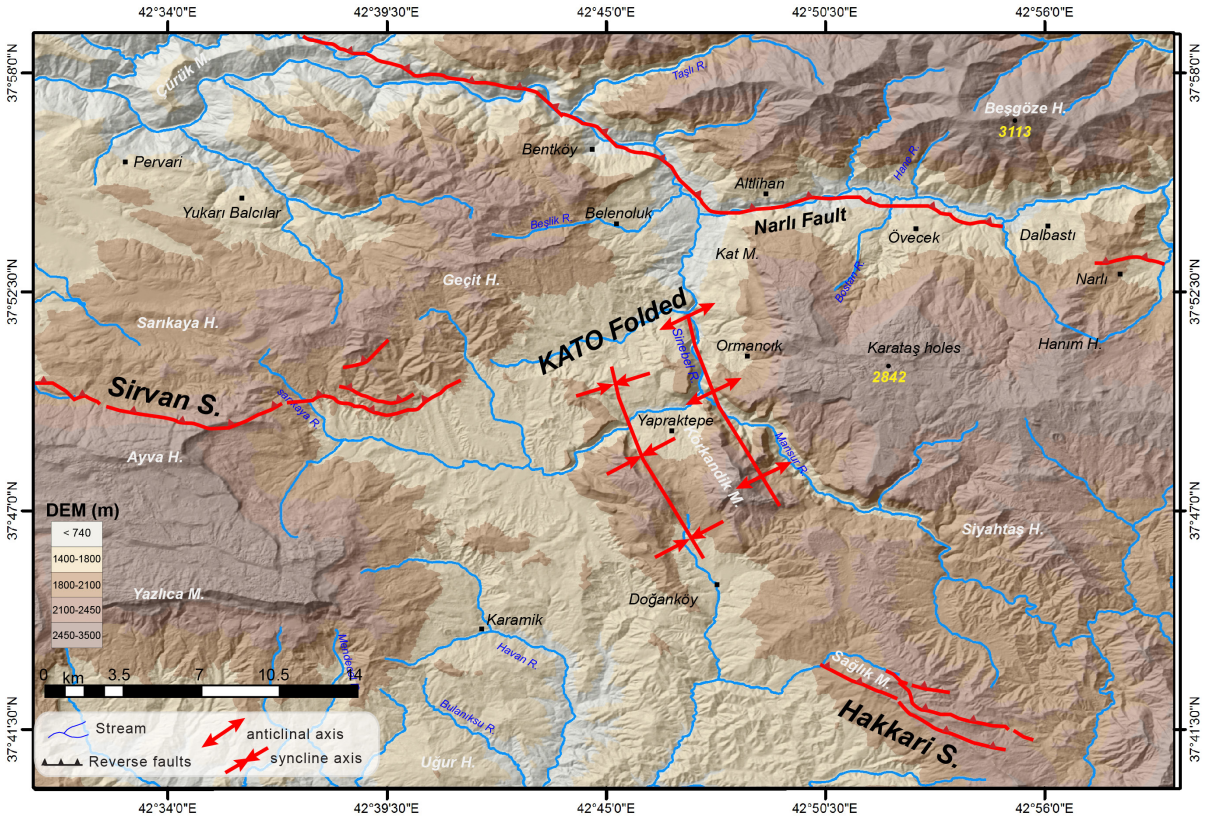


**Figure 4.** Active faults and folds of the middle of BZFTB in Turkey (faults from Emre et al., 2013).

Tectonic evolution of the region has resulted in frequent, short-range facies changes and stratigraphic unconformities forming across horizontal and vertical planes in the study area and its immediate surroundings. In the Imbricated Zone Triassic-Quaternary units are present (Figure 2). Clastic and carbonate rocks of Cretaceous-Eocene age crop out in the study area (Figure 2). Permian crystallized limestone, marble and calcschist cover other units in the form of nappes (Aktürk, 1985). The units, characterized by Eocene-Miocene sandstone and marl intercalations, are turbiditic sediments and commonly outcrop in the study area (Perinçek and Özkaya 1981; Perinçek, 1990). While Upper Triassic-Lower Cretaceous strata are only coming out in the core of some anticlines, most anticlines involve Cretaceous carbonate rocks, and Tertiary clastic rocks are protected within the side-by-side synclines (Zebari et al., 2019). Unconsolidated Quaternary deposits such as alluvial fan deposits, slope sediments and river terraces are extensively exposed throughout the Sinebel Valley in the study area.

## 3. Materials and methods

We carried out this research in two stages, simply as a field and geomorphic indices study. We calculated and analyzed geomorphic indices from DEMs for the BZFTB in the study area and based on the literature data and new field observations, the landscape evolution model of the study area was created.

### 3.1. Field studies

We conducted a standard field study, collecting structural data related to deformation. We analyzed the all structural data measured at different locations around the Sinebel Valley using rose diagram. All data were computed using the Stereonet 11 (https://rickallmendinger.net/). For each structural data, (a) plane direction (b) dip direction, (c) dip amount and (d) rate referring to the quality of the measurement were evaluated. Thus, we had the possibility to compare the general trends of the folds that developed in the region.

### 3.2. Morphometric indices

Various studies in recent years show that events in deformation zones leave multiple topographic traces on the landscape (Bull, 1977; Keller, 1986; Gordon et al., 1998; Keller and Pinter, 2002; Giamboni et al., 2005). Morphometric analysis is one of the methods used to evaluate these traces on the earth surface. In tectonically active regions, the drainage system is used both quantitatively and qualitatively to investigate the tectonic evolution and geomorphic processes (Jackson et al., 1998; Sung and Chen, 2004; Delcaillau et al., 2006; Ramsey et

al., 2008; Bahrami, 2013). These analyses are made by using geomorphic indices to understand the topographic evolution of large areas or to define the degree and timing of activity on fault segments (Strahler, 1952; Bull and McFadden, 1977; Keller et al., 2000; Azor et al., 2002; Keller and Pinter, 2002; Font et al., 2010).

This study utilized the geomorphic indices of hypsometric curve and hypsometric integral (*HC, HI*), surface roughness (*SR*), steepness index (*Ks*) and normalized channel steepness index (Ksn) (Table). Topographic and morphometric analyses were made by using ArcGIS software to analyze the DEM produced from 1/25,000 topographic maps of the study area. A homogeneous data set was obtained by filling data gaps in the DEM by interpolation (Fill Sinks tool, etc.). The drainage basins and river network of the region were created on the base of the DEM, and these river networks were compared with the networks on topographic maps. Arc Hydro tool was used for drainage basins and

**Table.** Average values of the morphometric parameters for the various scarps and drainage basins.

| Geomorphological features | Area 1 | Area 2 | Area 3 |
|---|---|---|---|
| | Şirvan Segment | Transfer zone | Hakkâri Segment |
| Number of basin | 21 | 21 | 19 |
| Hypsometric curve and integral (*HC* and *HI*) (1) | 0.412 | 0.62 | 0.465 |
| Surface roughness (2) | 1.28 | 1.43 | 1.30 |
| Swath profiles (3) | 4 | 3 | 6 |
| Steepness index (4) | 425 | 180 | 350 |
| Normalized channel steepness index (*Ksn*) (5) | 525 | 156 | 425 |

(1) This analysis, consisting of two different values, is specified as hypsometric curve and hypsometric integral. The hypsometric curve (*HC*) provides information about the evolution of basins with elevation differences from the drainage area in a region and the erosion of the landscape (Strahler, 1952). Hypsometric curve characterizes the basin while hypsometric curve with a convex curve is young (*HI* > 0.5), immature, and less erosion process compared to other basins, while the S-shaped hypsometric curve indicates midmaturation phase and moderately eroded basins (0.3 < *HI* < 0.5), Concave shaped curves indicate that the maturation phase is completed, old and erosion activities are high (*HI* < 0.3) (Keller and Pinter, 2002; Pérez-Peña et al., 2009a; Giaconia et al., 2012). The hypsometric indices calculated in this study were used in the CallHypso software (Pérez-Peña et al., 2009a,b) operating under the ArcGIS software.
(2) Surface roughness (*SR*) measures how much an area digresses from being entirely flat. A flat, planar surface has a surface roughness value close to one, while irregular surfaces have values greater than one, increasing as there is more erosion and incision by streams. This index is calculated by the SR = TS/FS equation (Hobson, 1972, Grohmann, 2004), where TS is the areas ($m^2$) of the actual topographic surface and FS is the projection of the surface corresponding to a planar surface.
(3) Swath profiles are projected profiles where evenly spaced profile lines cross the contours within a swath (Baulig, 1926). In fact, Swath profile analysis is accepted a developed digital elevation model-based version of the traditional crosssection analysis (Usta, 2015). In a SWAT profile area and elevation data are recorded along vertical lines to the profile line (Usta, 2015). These elevation data consist of calculating minimum-highest and average values (Hergarten et al., 2014). Topographic swath profile analysis can be a useful tool in tectonic studies (Telbisz et al., 2013), because there is a need to define and measure the difference between the topographies affected by the segments. Fault morphological structures such as sudden slope fractures, fault front plains can be clearly defined in elevation profiles.
(4) The steepness index (K*s*) is calculated directly by regression of the slope and area data (Montgomery et al. 1996; Homke et al., 2004; Whipple, 2004; Wobus et al. 2006). These areas and slope values are calculated from the area-slope graphs of the selected streams. For the same upstream region, the slope of a low-uplift flow is lower than the gradient of a high-uplift flow. The different uplift rates or decrease in erosion rates in the region may cause an abnormal increase in steepness (K*s*) values (Snyder et al., 2000; Kirby and Whipple 2001; Vanlaningham et al., 2006).
(5) Normalized channel steepness index can be used as a reference system to evaluate the causes of a river breaking suddenly while flowing in equilibrium (Ouimet et al., 2009; Whittaker, 2012). The use of the normalized channel steepness index (*Ksn*) resulting from the slope-area relationship (due to withdrawal) is widely used to identify regions subjected to different rock uplift rates (Wobus et al., 2006; Kirby and Whipple, 2012). Rivers under the influence of tectonism show high slopes. The normalized channel steepness index facilitates the comparison between different tectonic environments (Safran et al., 2005; Wobus et al., 2006; Cyr et al., 2010). Factors such as the erosion coefficient of rocks are influenced by the river-power law, such as different rock types through which rivers pass or climatic signs such as glaciers (Whipple and Tucker, 1999). While high normalized channel steepness index (*Ksn*) values indicate areas exposed to tectonism, it indicates that there are high erosion rates and rivers with high slopes (DiBiase et al., 2010; Kirby and Whipple, 2012). In this study, *Ksn* was calculated using the TecDEM toolbox developed by Shahzad and Gloaguen (2011).

river network. The steepness index (*Ks*) and normalized channel steepness index (*Ksn*) values were calculated with the TECDEM 2.0 (Shazad and Gloaguen, 2011). These plots constitute very useful tools when analyzing river knickpoints and can be used to differentiate migrating or vertical-steep knickpoints from slope-break knickpoints that separate areas with differential uplift (Wobus et al., 2006; Burbank and Anderson, 2012; Kirby and Whipple, 2012; Whipple et al., 2013). Depending on these values, relative uplift rate maps of the region were trying to be created. In addition, the created this interpolation map was created using the inverse distance weighted (IDW) and kriging interpolation technique in the ArcGIS program.

## 4. Results

### 4.1. Segmentation and deformation characteristics of the Şirvan and Hakkâri Segments from the field studies

The Şirvan Segment controls west of the study area and in some areas (in the northwest) it is observed that the Şirvan Segment has a dextral strike-slip component (Emre et al., 2013). The Şirvan Segment makes a right-lateral stepover around the Düğüncüler Village and continues eastwards as the Hakkâri Segment (Figure 3). The Şirvan Segment is a north dipping thrust fault in the N80°W direction with a dextral strike-slip component. When followed along the segment, it makes a concave turn around Pervari and continues as a pure thrust fault. Therefore, the hanging wall block in the western part of the segment has a flatter topography, while the eastern part has more rugged topography.

The western end of the Hakkâri thrust fault has a right-lateral component in the N80°-85°W direction and is composed of three subparallel segments, each one is 4–8 km in length, resulting in rough topography. The eastern part of the Hakkâri Segment has a pure thrust component in the E-W direction with rough topography on the footwall and flatter topography on the hanging wall.

From the onset of a collision, the deformation front of BZFTB has expanded 250–350 km south-west, transforming the margin into in NW-SE trending foreland fold-thrust belt (Mouthereau et al., 2007; Zebari et al., 2019). With the continuation of N-S compression in the region, transfer zones developed in the areas where the fault splay (Şengör et al., 1985). The Şirvan Segment of the BZFTB located in the north of the study area continues as the Hakkâri Segment by overstepping approximately 15 km to the right. According to some tectonic models proposed for the region, normal faults and extension fissure have developed in the areas where the faults step to the right due to N-S compression in the region (Şengör et al., 1985). This area between the Şirvan and the Hakkâri Segments is the transfer zone and controlled by the normal faults with an approximately N15°W direction.

### 4.2. Kato Folded and Sinebel Valley

Tectonic activity primarily affects and controls basin development and river-valley morphology with erosion and depositional processes (Nicol, 2010). The general topographic structure of the western part of BZFTB in Turkey started to develop with N-S compression during the middle-late Miocene (Hempton, 1985; Dewey et al., 1986; Robertson, 2000; McQuarrie et al., 2003; Şengör et al., 2003, Şengör and Natal'in, 2004; Al-Lazki et al., 2004). Most of the topographic features within the region trend in an E-W direction and the region is drained by multiple streams that form part of the catchment of the Euphrates and Tigris rivers.

Topographic features that developed in different directions are present in the study region between the Pervari-Beytüşebap (Eastern Anatolia) (Figure 3A). There are three remarkable macrotopographic structures in this region: (i) Kato Mountain (2842 m elevation) (Figure 3B), (ii) Sinebel Split Valley (Figure 3C), and (iii) Mount Körkandil (2779 m elevation) (Figure 3B).

Kato Mountain, on the eastern side of the study area, extends approximately N-S trend with a karstified plateau in its upper reaches. The western slope of this mountain is a cliff formed under fault control in the direction NNW-SSE, and is one of the most important topographic features in the field. The altitude of this cliff is around 800 m and it has a slope angle of 85–90° (Figure 3B).

Sinebel Valley, which is deeply eroded by Sinebel River, lies to the west of the cliff (Figure 3B) and is one of the narrowest and deepest valleys in the region (Zorer and Öztürk, 2021). Sinebel Valley contains one of the rare streams that flows towards the north within the Tigris River drainage basin. This valley trends NW-SE until Mount Körkandil, and thereafter turns 45° east and continues in the N-S direction (Figure 3). After leaving this valley, the stream turns westward at an angle of approximately 45° in the direction of flow, trending NW-SE. The length of the valley is approximately 10 km and its base-width decreases from south to north to a few meters in the lower parts of the valley in the north. The depth of the valley is much greater in the southern Mount Körkandil region compared to the north, where it reaches a maximum depth of 375 m. This morphology is important in terms of the formation and development of the valley. Terraces, which are formed due to the rise on the slopes of the valley, extend as four main steps along the slope (Figure 3C). The Sinebel River Valley adopts the morphology of an "ingrown meander" after Mount Körkandil, where it changes direction and continues flowing northwards (Figure 3A).

Mount Körkandil in the southwest of the study area is the second highest peak in the region with an altitude of 2799 m. The degree of the eastern, western and southern slopes of the mountain is high. The eastern shoulder of the mountain reaches Sinebel Valley, where the lower parts of

the shoulder form a portion of the western shoulder of the valley (Figures 3A and 3B).

Some of the most important structures that are formed by the forces causing deformation are the folds. Folds provide clear information about the geodynamic evolution of the zone (Burbank and Anderson, 2012). In the study area, anticlines and synclines, locally as the Kato Folds, contain more than one folding axis (Figure 5). These folds were developed in the Eocene clastic units and Cretaceous thickly bedded limestone units (Figures 5A and 5B). While the bedded slopes of the limestone unit are at a lower angle around Mount Körkandil, they are close to perpendicular in the northern part of the study area (Figures 5B–5D). The directions of the folding axes are parallel to the Sinebel Valley and generally have a direction of N10°-20°W (Figure 5).

The results of the stress analyses applied to the folds provide information on the main stress directions that will form the folding. In the field study, bedded measurements were taken in the areas where limestone and turbiditic sediments crop out (Figure 6A). Dip and strike measurements of approximately 49 bedding in Sinebel Valley were processed in stereonet software and rose diagram analyses were performed (Figures 6B and 6C). When the locations of these bedded were added to the stereonet, it was observed that the orientation of the folds axes in this area was dominantly NW-SE (Figures 6B and 6C). When the bed dips and strikes measured across the anticlinal and synclinal axes were evaluated individually, it was found that the direction of the Kato anticline is N19°W and the direction of the syncline is N24°W (Figures 6B and 6C). Furthermore, it was observed that these folds axes

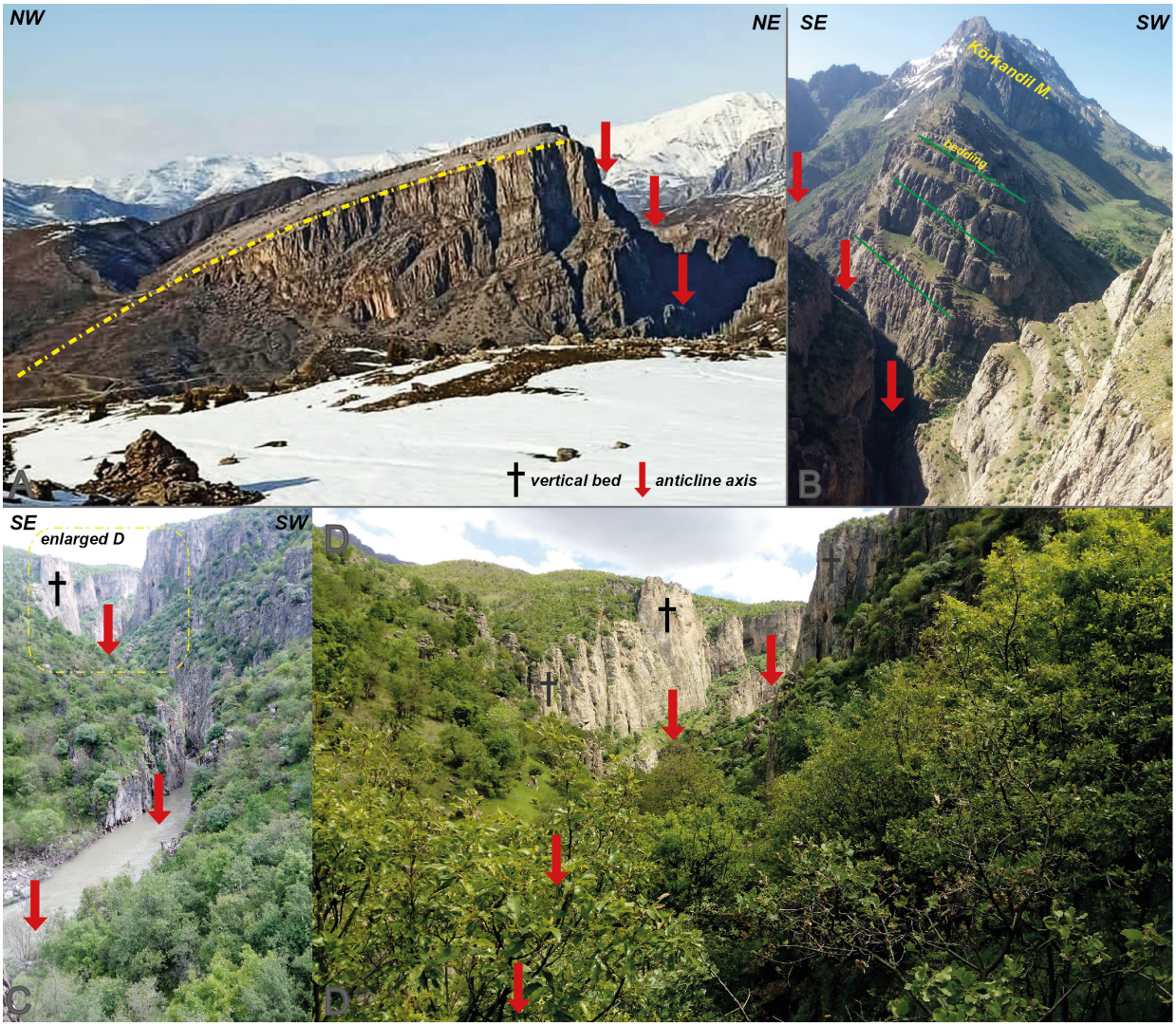


**Figure 5.** A) The fold limb developed on the western shoulder of Mount Körkandil, B) the fold limb, C) the beds that are close to vertical on the eastern shoulder of Sinebel Valley, D) the appearance of the vertical beds across the valley.

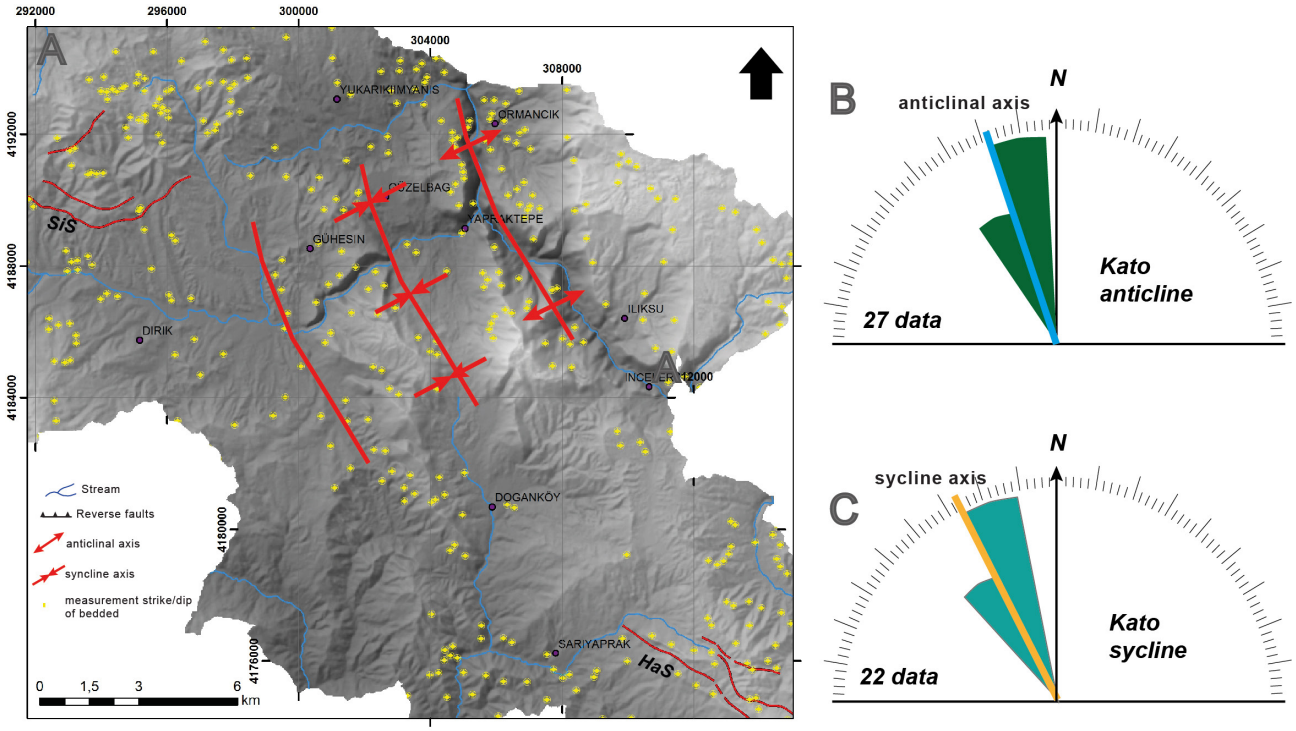


**Figure 6.** A) Locations of dip and strike measurements of the beds obtained across the study area, B) stereonet analysis of the Kato anticlines, C) stereonet analysis of the Kato synclines.

dipped towards the northwest and had undergone a severe deformation in some parts. As a result of the analyses, it was seen that the main stress direction to form the Kato Folds was NE-SW.

### 4.3. Geomorphic analysis

The study area was divided into three sectors; Area 1, Area 2, and Area 3, according to the segmentation of faults. The Şirvan Segment (Area 1) extends to the west and the Hakkâri Segment (Area 3) controls the eastern part (Figure 7). Area 2 is a transfer zone in the area where these faults stepover. Sixty-one subbasins have been defined in river catchments in the study area (Table).

#### 4.3.1. Şirvan Segment (Area 1)

This analysis provides information about the evolution of basins with elevation differences from the drainage area in a region and the erosion of the landscape (*HC-HI*), in identifying surfaces eroded and interrupted by currents (*SR*), in determining the difference between topographies affected by segments (Swath), the different uplift rates or decrease in erosion rates in the region (*Ks-Ksn*).The hypsometric index shows the abrasion-erosion relationship developing in a basin as a result of active tectonism (Strahler, 1957, Keller and Pinter, 2002; Pérez-Peña et al., 2009a; Giaconia et al., 2012). The HI values and HC curve of 21 different drainage basins along the Şirvan Segment and area1 were calculated (Table). These HI values range between 0.34 and 0.64 (Figure 7A, Table). The *HI* values in the northern hanging wall block of the Şirvan Segment are lower, while the *HI* values in the southern footwall block are higher. The shapes of the hypsometric curves are different between subbasins located in these areas (Figure 7B). While the curves of the footwall basins of the Şirvan Segment are convex-shaped, the curves of the hanging wall basins are S-shaped (Figure 7B), indicating the footwall basins are young and immature, while the hanging wall basins have completed their development and are now exposed to erosion (Figure 7B).

On the contrary, surface roughness values have different values in the hanging wall and footwall along the Şirvan Fault (Figure 8). The lowest values of *SR* were obtained in the northwestern and eastern part of Area 1 (Figure 8).

Especially in the northwest, where the Şirvan Segment has a low right-lateral component, it has high *SR* values in the south. High roughness values have again observed in the eastern parts of the hanging wall block (Figure 8).

The topography of the footwall and hanging wall are one of the important factors in revealing the tectonic-topography relationship. The effect of the active fault on the topography can be observed in the profiles taken across the Şirvan Segment (Figures 9U1–9U4). The footwall at the western end of the segment has a flat topography with 2000

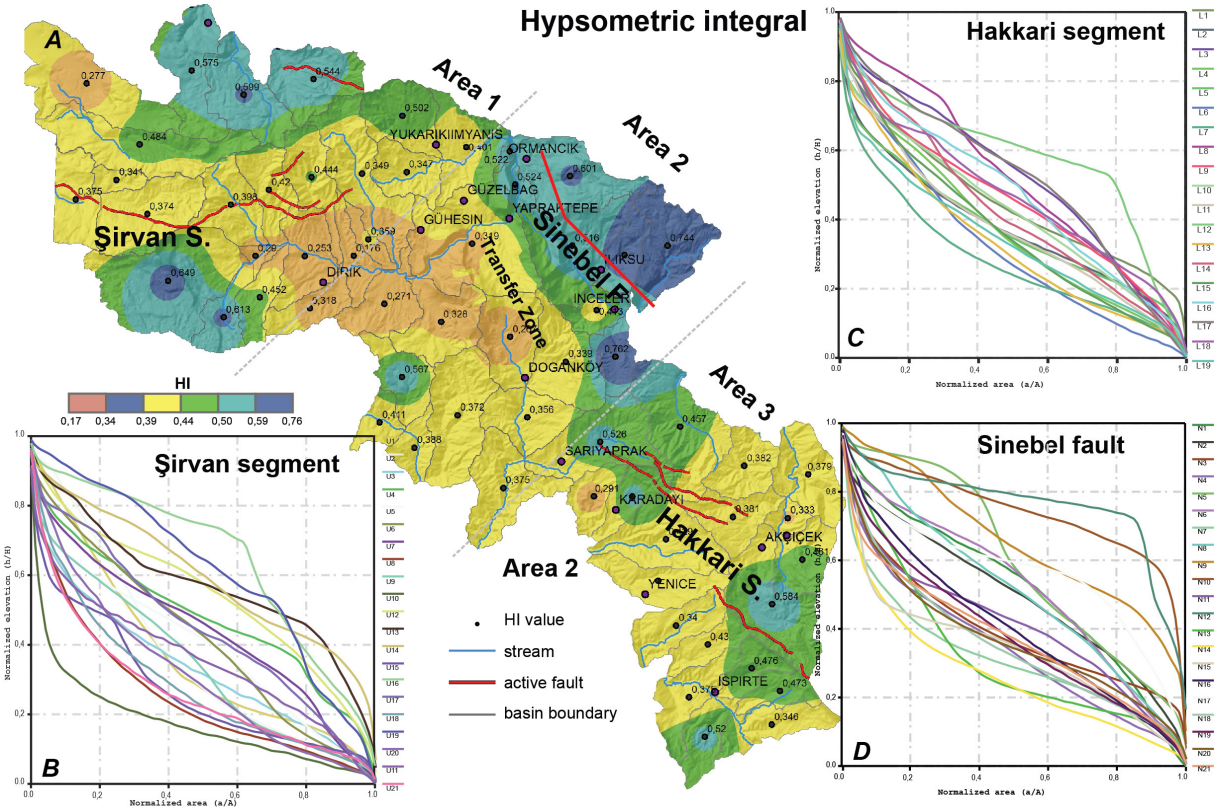


**Figure 7.** A) The interpolation map of the study area related to hypsometric integral values, B) the **Şirvan** Segment, C) the Hakkâri Segment, D) the Sinebel Fault.

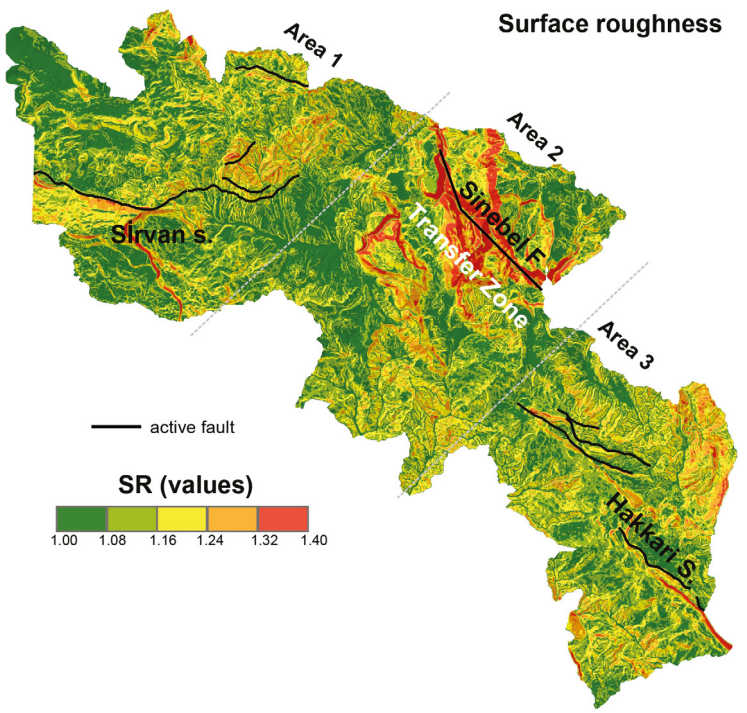


**Figure 8.** The surface roughness (*SR*) values of the study area.

m elevation, while the altitude of the hanging wall reaches 2700 m due to thrust faulting (Figure 9U1). In the eastern part of the Şirvan Segment, a more complex topography was observed, as can be seen in U3 and U4 profiles (Figure 9) where there are multiple knickpoints resulting from the scattered structure of the segment in this area. Especially in the east of this segment, in areas controlled by small but parallel faults, it can be said that the deformation due to the rise in the hanging wall is more.

The highest normalized steepness index values (*Ksn* > 400) were observed in the Imbricated Zone and to the north of the Şirvan Segment, these values indicating the highest uplift. In the north and especially the east of Area 1 the steepness values are high, while they are moderate in the middle sections (Figure 10A). It is seen that the *Ksn* values calculated based on the steepness index and concavity values are compatible with other results. The values of *Ksn* are between 75 and 680 in the region defined as Area 1 (Table). The *Ksn* values of the stream channels in the northern part of Area 1 were lower (>100), while they increased to the south (Figure 10B). *Ksn* values in the uplifted block north of the Şirvan Segment were <400,

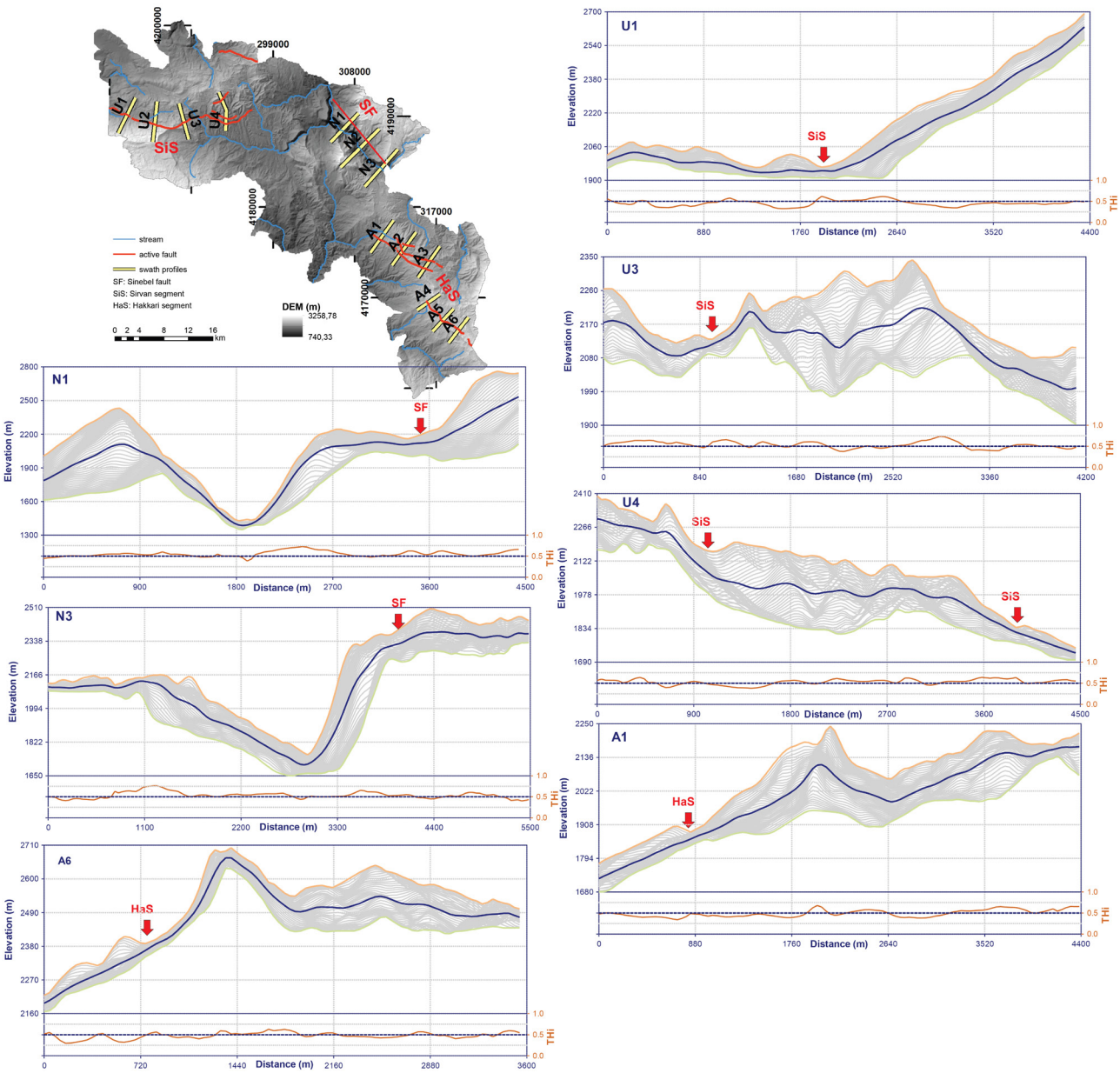


**Figure 9.** The locations and profile sections of the swath profiles perpendicular to Şirvan, Sinebel, and Hakkâri segments of the BZFTB.

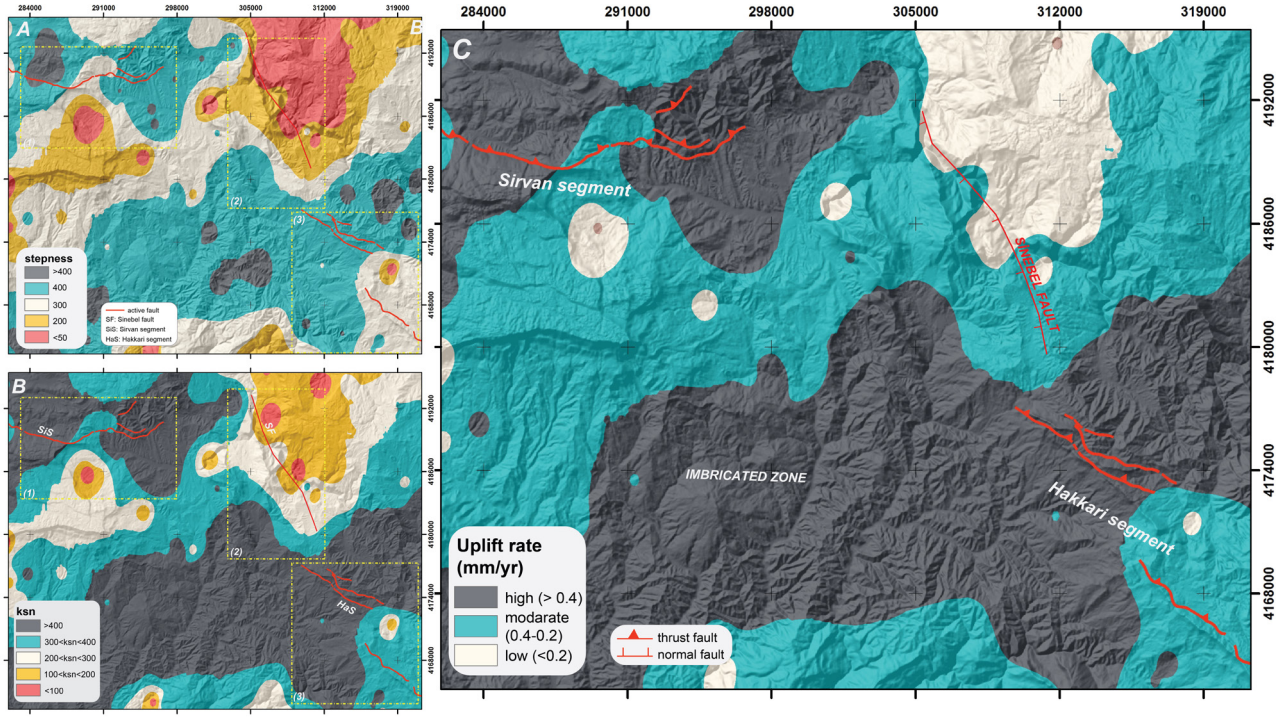


**Figure 10.** A) Interpolation of steepness index values, B) the sensitivity map of *Ksn* against current tectonism, C) relative rising ratios related to geomorphic indices, of the study field.

while the values were <100 in the middle of the footwall block (Figure 10B).

A relative uplift map of the region was derived by analyzing knickpoint, channel steepness, and steepness indices (Figure 10C). According to Figure 10C, the areas with a relative high uplift rate are to the north of the Şirvan Segment and the southern part of the study field. The relative uplift rate of these areas is estimated to be greater than 0.4 mm year$^{-1}$. The high erosion rate observed in the footwall block of the western Şirvan and in the hanging wall block in the east shows that the deformation along the BZFTB changes depending on the stress components of the fault.

### 4.3.2. Hakkâri Segment (Area 3)

In the Hakkâri Segment the *HI* values of the basins in the southeastern part of this segment are between 0.34 and 0.59 (Figure 7A, Table). In the northwestern and southwestern parts of the segment *HI* values are between 0.44 and 0.50, and in the middle parts, the *HI* values are between 0.39 and 0.44 (Figure 7A). These values suggest, basins on either end of the Hakkâri Segment are immature, while basins in the middle of the segment are mature and are now exposed to erosion (Figure 7C). However, it is seen that surface roughness values and hypsometric curve graphs are compatible with each other. Surface roughness values of the Hakkâri Segment vary between 1 and 1.43. While *SR* values are high, especially along the fault line, it is seen that these values decrease as they move to the northeast and southwest (Figure 8). The *SR* value is maximum at the southeast edge of the segment. (Figure 8).

The topography in the 2-D swath profiles taken along the Hakkâri Segment is rougher compared to the other areas of the study field (Figures 9A1 and –9A6). Although the steepness of the fault can be seen clearly, the average altitude changes from A1 to A6. The relief is around approximately 300 m (A1) in the northwest parts of the hanging wall, where the slope increases. However, this difference decreases to approximately 100 m (A6) in the southeast parts. The location of the active fault is clearly observed in swath profiles perpendicular to the along of the Hakkâri Segment. In areas where there are more than one knickpoint in the hanging wall along the profiles, it is probably due to small faults located in these areas. According to in the normalized steepness index analysis, the highest values in the study area were obtained from this area defined as Area 3 (Figure 10A).

The high *Ksn* values in the northwestern part of Area 3, which contains the Hakkâri segment, show that this area also has an estimated relatively high uplift rate. In the southeastern part of this area, these values are moderate, and this area has experienced moderate relative uplift rates (Figure 10A). A zone *Ksn* index difference draws attention to the transfer zone between the Şirvan and Hakkâri

Segments. This zone is in the NW-SE direction and the *Ksn* values are between 200 and 400 (Figure 10B).

In Area 3, which is controlled by the Hakkâri Segment, the northwest sections have low *Ksn* values (100 > *Ksn*). *Ksn* values are higher in the south where Hakkâri displays a right-lateral offset (Figure 10B). In the other parts of the Hakkâri Segment, *Ksn* values are between 100 and 200. A relative uplift map of the region was derived by analyzing knickpoint, channel steepness, and steepness indices (Figure 10C). According to Figure 10C, the areas with a relative high uplift rate are to the north of the Hakkâri Segment. The estimated uplift rate of these areas is greater than 0.4 mm year$^{-1}$.

#### 4.3.3. Transfer zone (Area 2)

Hypsometric curve and integral values that clearly show the erosion developing in the transfer zone between the segments is rather different. The *HI* values of this area vary between 0.34 and 0.76 (Figure 7A). The *HI* values in the northeastern part of this area that is controlled by the Sinebel Fault are between 0.50 and 0.76. In the southwestern parts, the *HI* values are between 0.50 and 0.76, while in the middle sections *HI* values are the lowest (0.34) (Figure 7A). In this area, where the Kato anticline is present, the basins have convex-shaped hypsometric curves indicating they are immature basins (Figure 7D). Only the basins in a very narrow area in the middle part of the area can be classified as mature (Figure 7D).

The highest surface roughness values in the study area are seen in the transfer zone between the Hakkâri and Şirvan Segments (Figure 8). It was observed that the *SR* values of the areas parallel to the direction of the Kato Folds and Sinebel Valley were high (Figure 8). It is observed that these values are particularly high on the western slopes of Mountain Kato, which limits the eastern part of the study area. Once again, these values are also very high in the Bent stream flowing in the same direction with the Sinebel Valley in the west (Figure 8).

The transfer zone has asymmetrical slopes perpendicular to the Sinebel Fault in a N20°W direction and where the eastern end of the Şirvan Segment (Figures 9N1 and 9N3). While the bottom of the valley has an altitude of 1450 m, the altitude of the east slope is around 1825 m (maximum) (Figure 9, N1). In the profiles taken perpendicular to the transfer zone, the piedmont developed in the hanging of the normal fault, called the Sinebel Fault, are clearly seen. The piedmont (1100 m length) developed across the Sinebel Fault is located at the northwest of the fault (N1) and the fault front plane at the southeast is at a higher altitude (N3) and located in a narrower area (475 m length) (Figure 9N).

Steepness index analysis, which is used to understand the relative uplift ratios, is located in the low-medium values in Area 2, which includes many morphological and structural structures. Minimum Ksn values were obtained in the hanging wall of the Sinebel Fault (Figure 10A). Maximum values in this area are located at the northern and southern ends of the Sinebel Fault. In fact, these values originate from the ends and starting points of thrust faults controlling the area (Figure 10A). It is seen that normalized channel steepness (Ksn) and steepness index calculated for this area are compatible with each other. *Ksn* values were lower in Area 2 which is located in the middle of the study area. The values were between 200 and 500, with low values observed across the Sinebel Valley (Figure 10B).

Area 2 containing the Sinebel Valley and the Kato Folds has relatively lower uplift rates (<0.2 mm year$^{-}$1). The areas that have an uplift rate between 0.2 and 0.4 were considered as moderate uplift areas and are almost parallel to the direction of the areas with a high uplift rate (Figure 10C).

## 5. Discussion

New tectonic regime started with the collision of the Arabian and Eurasian plates during the late Miocene-early Pliocene and a change in stress direction to N-S (Şengör et al., 1985; Kelling et al., 1987). Along with the collision, depending on the tectonic regime change in the region, the stress directions affecting the region have changed and the directions of the main structural controlling the deformation have varied. The effects of this differentiation are clearly visible on the morphology.

### 5.1. Main stress direction estimate using dip and strike measurements

Previous studies carried out in the region (Şaroğlu et al., 1987; Emre et al., 2013) defined the thrust faults and folds that formed during paleotectonic activity, generally trend NNE-SSW. In addition, Şaroğlu et al. (1987) stated in his study that the general strikes of extend and thrust faults of the paleotectonic period in the Pervari-Beytüşebap region are in the NNE-SSE direction. However, according to the folding analysis results indicated for the Kato Folds, the compression regime is in the NE-SW direction before the collision. The Kato Folds also trend NNW-SSW, indicating the region was compressed in the N60°E direction during the Pre-Oligocene (Figure 11A). Anticlines and synclines with 12 km long fold axes were developed as a result of this compression. Nevertheless, with the effect of the Neotethys Ocean, a flatter topography started to dominate with the sediment accumulation in these folded areas in Miocene.

### 5.2. Reconstructions with topographic evolution of Hakkâri and Şirvan Segments

BZFTB is one of the most important deformation structures formed due to the N-S compression regime controlling the region. With the deformation evolution of the BZFTB, the topographic development of the region started to change after the Pliocene (Zebari and Burberry, 2015; Zebari et al., 2019). The faults in this suture zone are mostly low-angle

thrust faults that developed as a result of the collision and are cut by the left-lateral strike-slip East Anatolian Fault (EAF) in the west. While the faults on its western half were developed within a narrow zone, the faults on its east have dispersed over a wider zone (Duman et al., 2017). The part of BZFTB within the borders of Turkey is divided into 12 different segments (Emre et al., 2013). In the study area, the Şirvan and Hakkâri Fault Segments, which form the northern and southern boundaries of the Imbricated Zone, respectively, are with trends between N80°-85°W and E-W (Figure 11B). Transfer zone approximately 20 km wide with a right-lateral stress component is present to the south of the Çatak district (Van) between the Şirvan and Hakkari Segments (Figures 2 and 3) where extension deformation structures are observed (Figure 11B).

Actually, a complex deformation structure as BZFTB is often treated as a single structure. This complex fault system will necessarily accommodate both strike-slip and dip-slip motions (Reilinger et al., 2006), in fact deformation is likely partitioned between different structures (Talebian and Jackson, 2002). It is also stated that extensional structures develop between thrust faults in the Eastern Anatolian compression region (Şengör et al., 1985). Mountain chains in the E-W direction and opening fractures in the N-S directions were formed due to this compression (Şaroğlu and Güner, 1981). At the same time, due to this local E-W extension, normal faults perpendicular to the compression direction were formed (Figure 11C). One of these deformation structures is the transfer zone that controls the redevelopment of the Sinebel Valley (Figure 11C).

The Şirvan Segment of the BZFTB located in the north of the study area continues as the Hakkari segment by leaping approximately 15 km to the right. According to some tectonic models proposed for the region, normal faults and extension fissure have developed in the areas where the faults step to the right due to N-S compression in the region (Şengör, et al., 1985). This area between the

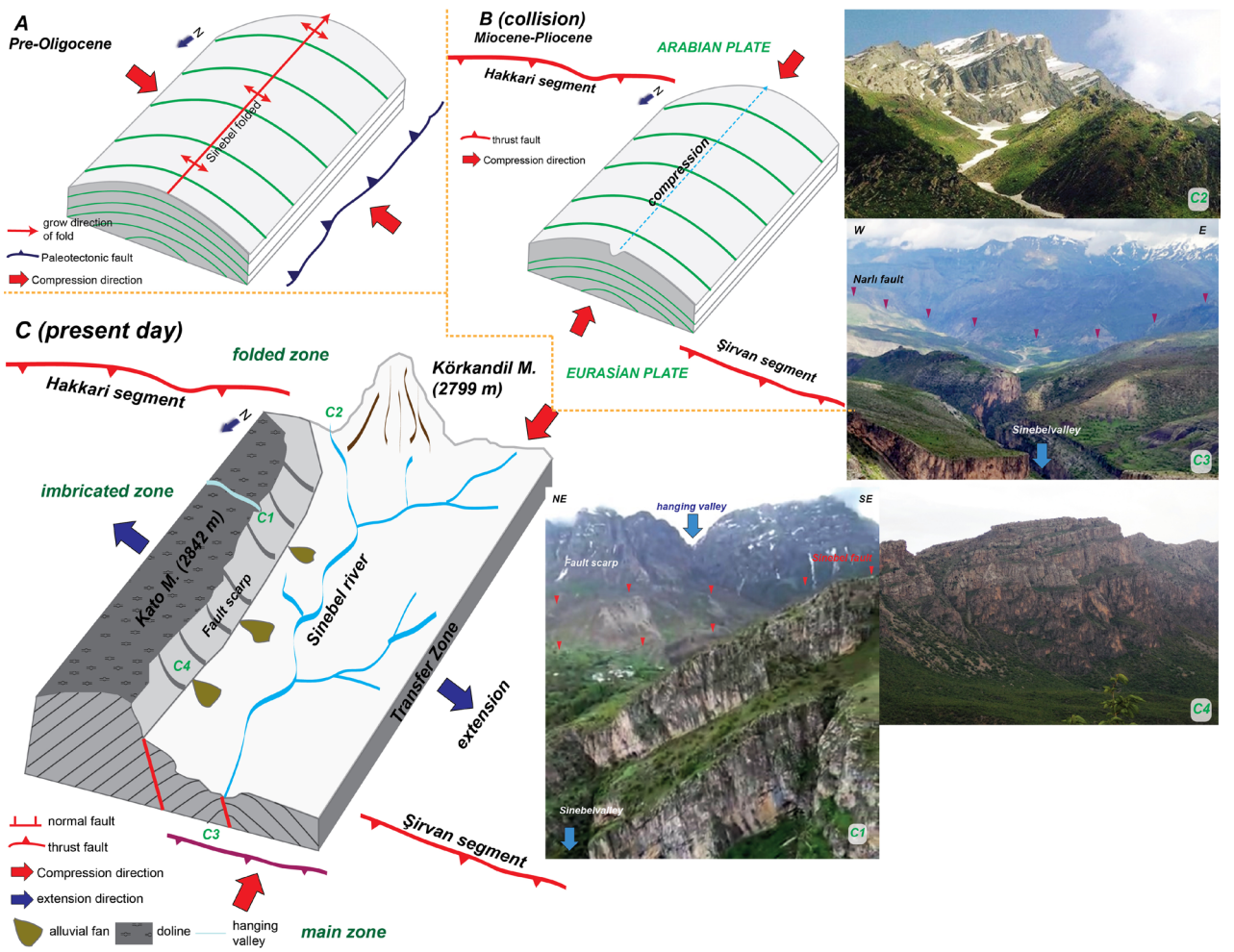


**Figure 11.** Topographic evolution of the study zone, A) Pre-Oligocene, B) Miocene-Pliocene, C) present-day topography of Sinebel River and its surroundings.

Şirvan and the Hakkari Segments was the transfer zone and normal faults controlled by the approximately N15°W direction were determined.

Especially, revealing the interaction of tectonic and erosion processes plays an important role in determining the landscape evolution in active orogenic belts (Siddiqui et al., 2017). One of the reasons for the significant change in erosion rates is any relative change in the base level caused by tectonics or climate (Zebari et al., 2019). A residue landscape stays when its uplift is not entirely balanced by erosion (Burbank and Anderson, 2012; Pérez-Peña et al., 2015; Andreani and Gloaguen, 2016). The most of studies from throughout the world indicate that the long-term uplift and exhumation rate due to tectonics is the primary control of short-term erosion rates (Blanckenburg, 2005). Moreover, Granger and Riebe (2007) conclude that cosmogenically derived erosion rates and long-term exhumation rates from thermochronometry indicate tectonics is far more important than climate in controlling erosion rates. In order to evaluate short-term erosion rates in the Şirvan Segment, Hakkâri Segment and Sinebel Valley quantitative geomorphic analyses have been conducted following the classical geomorphological approach. Due to the fact that the climate effect and the lithology are almost the same in the study area, the effects of tectonism on the erosion rate are discussed.

**5.3. Interpretation of uplift/exhumation rate in the Bitlis thrust zone belt**

It is known that the Eastern Anatolian High Plateau has been uplifted approximately 2000 m since the Middle Miocene (Serravallian) (Şengör et al., 1985). The exhumation of the BZFTB since the early Miocene has been modest (3–4 km), with average exhumation rates of 0.2–0.3 km $my^{-1}$ (Okay et al., 2010). Researches in recent years have shown that the rate of shortening is not the same across this plateau (Reilinger et al., 2006; Copley and Jackson, 2006). GNSS based geodetic studies suggest that the overall rate of shortening is also higher in the south and east of this region (Reilinger et al., 2006; Copley and Jackson, 2006). The shortening rate in the High Folded Zone and Imbricated Zone is around <2 mm $year^{-1}$ depending on the geological data (Allen et al., 2004), and based on morphotectonic analysis, the rate of uplift from south to north decreases (Sağlam Selçuk, 2016). Moreover, Sançar (2021) concluded that the spatial distribution of significant uplift within the western part of the Turkish-Iranian Plateau and signify the uplift rate is larger than the horizontal slip rate and the uplift rate in the Muş basin is higher than 0.5 mm $year^{-1}$. Within the scope of this study, it is seen that the relative uplift rate is high (>0.4 mm $year^{-1}$) for Hakkâri and Şirvan regions. The effects of this uplift are clearly observed, especially in the valleys in the study area. The steepness of the northern and southern slopes of the Sinebel Valley and the structural flatness which is formed on limestone bedding developed on these slopes are proof of more than one sudden uplift episode in this area (Figures 12A and 12B). In addition, the four terrace levels in the Sinebel Valley (Figure 12C) are evidence of the sudden uplift in these areas and show the accuracy of the uplift rates obtained within the scope of geomorphic analysis within the scope of this study. However, while the relative uplift rate is high along the Şirvan and Hakkâri Segments, this rate is much lower in the transfer zone region that develops between these segments.

**5.4. Development of the transfer zone**

Transfer zones are structures (fault, fold) that enable a smooth and regular variation in shortening between the overlapping ends of thrust faults (Dahlstrom, 1970). Faults on both sides of the transfer zone tend to dip in the same direction. This zone is where deformational strain is transferred from one structural element and divided on the basis of the dominant mode of deformation (Faulds and Varga, 1998). In their study, King and Yielding (1984) noted that thrust faults transmit deformation along normal faults in these stepovers.

The transfer zone (northwest of the Hakkâri) is composed of several smaller faults parallel to each other. The basins in this area are young and have a higher erosion rate compared to the southeastern part. Remarkably, the erosion rate is high in the areas controlled by the extension structure or normal faults and the basins in this area are young (Figures 13A and 13B). Moreover, Strak et al. (2011) stated that there was a positive correlation between the erosion rate and the normal fault, but the correlation between the distances to the fault was statistically insignificant. Due to the preferential erosion of highly fractured rocks, topographic lows and drainages may develop along the trace of transfer zones (Faulds and Varga, 1998). The topography was changed in the study area with the local extension and the Sinebel Valley started to flow in a N-S direction again. Likewise, in the southeastern parts of the BZFTB in the streams flowing parallel to this zone and with the folds develop parallel to the collision zone (Zebari et al., 2019).

The oldest erosion surfaces with the highest altitude are in the eastern part of the study at Kato Mountain and Mount Körkandil, between 2400 m and 2800 m. The peak of Kato Mountain is in the form of a karst plateau and contains hundreds of polygonal melting dolines. One section of the old drainage system is on this plateau surface and these valleys are in the form of a hanging valley formed due to E-W extension (Figure 11C). Studies in the Taurus Mountains determined these hanging valleys were mid-upper Miocene in age (Erol, 2001; Monod et al., 2006; Doğan et al., 2017).

In summary, with the closure of the Neotethys Ocean and active uplift of the region, erosional processes started to dominate again. The first topography that the

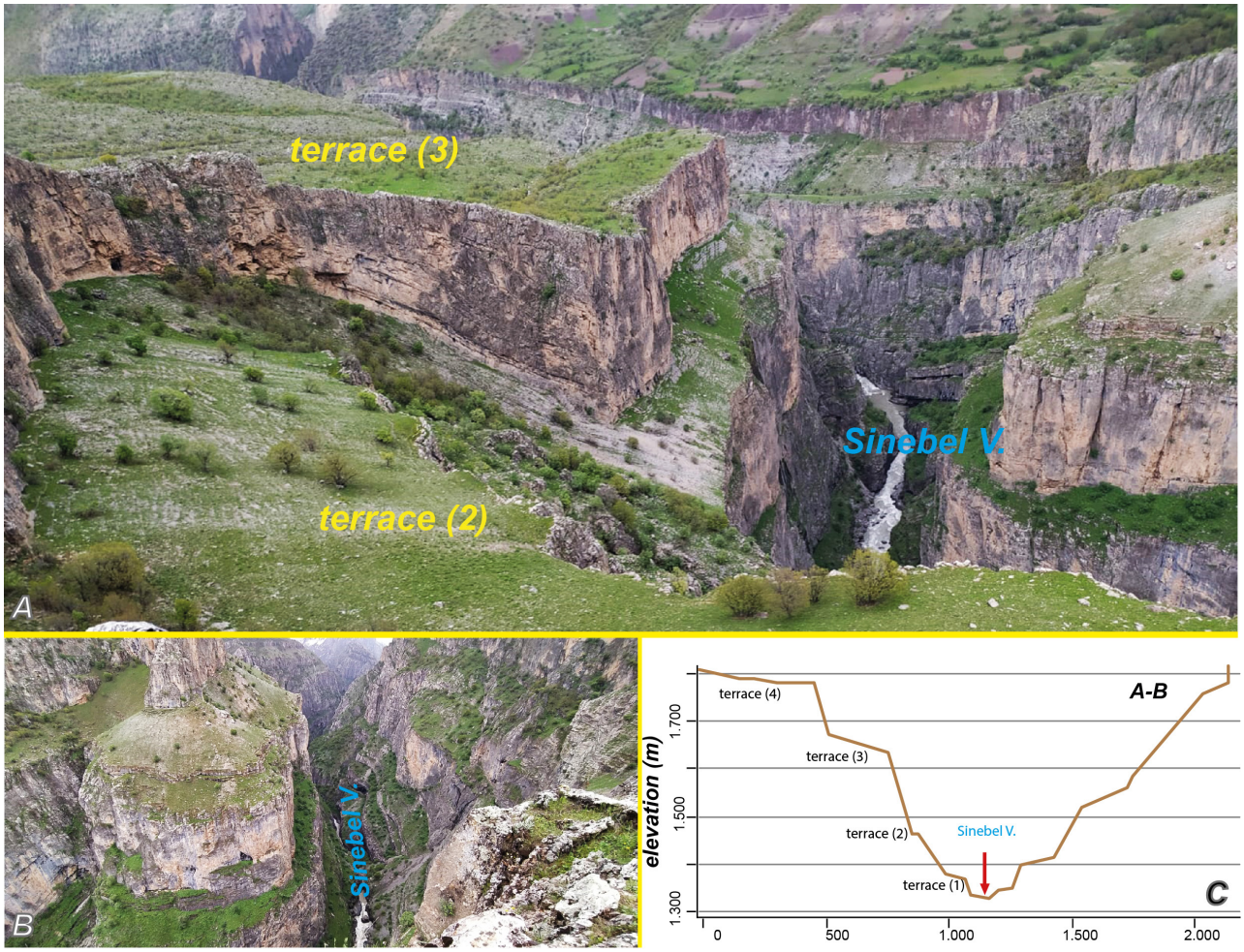


**Figure 12.** A) Levels of the terraces in the northern part of the Sinebel Valley, B) levels of the terraces in the south part of the Sinebel Valley, C) crosssection of the Sinebel Valley.

Sinebel River exploited had a low gradient and the river continued its flow in the N-S direction forming meanders. Generally, rivers react to regional uplift by down cutting to reequilibrate with base level (Davis, 1902; Schumm, 1993; Marr et al., 2000). The erosional forces of the Sinebel River exceeded uplift, hence it down-cut into the Kato Anticline, which was formed by the E-W compression during the Oligocene-Miocene. The hanging valley, which extends in the E-W direction and is perpendicular to the normal fault on Mount Kato, confirms this topographic development. Furthermore, regional uplift resulted in enhanced karstification with hundreds of dolines formed on Kato Mountain and Mount Körkandil (Öztürk and Zorer, 2020) (Figure 11C).

## 5. Conclusion

This study focused on a region between Pervari and Beytüşebap (East Anatolia) located in the northern part of the Bitlis-Zagros Fold-Thrust Belt, southeastern Turkey. The Hakkâri and Şirvan Fault, the Kato Folds and Sinebel Valley were analyzed to determine the effects of active tectonism on the topographic evolution of the region.

(i) This area experienced two compressional events in two different directions before and after the upper Miocene. Angular unconformites, terraces at different altitudes on the valley slopes, and fold axes that are noncompliant with the present-day compression direction are all indicators of the polyphase deformation history of this region.

(ii) The effect of the BZFTB on topography in this area continues at different times and under the influence of active faults with different characteristics. We can best see this on the temporal deformation of Mount Kato, Sinebel Valley and Körkandil Mountain, which are among the important topographic structures. A right-lateral transfer zone developed between the two fault segments, causing local extension and the Kato Folds to open in the E-W

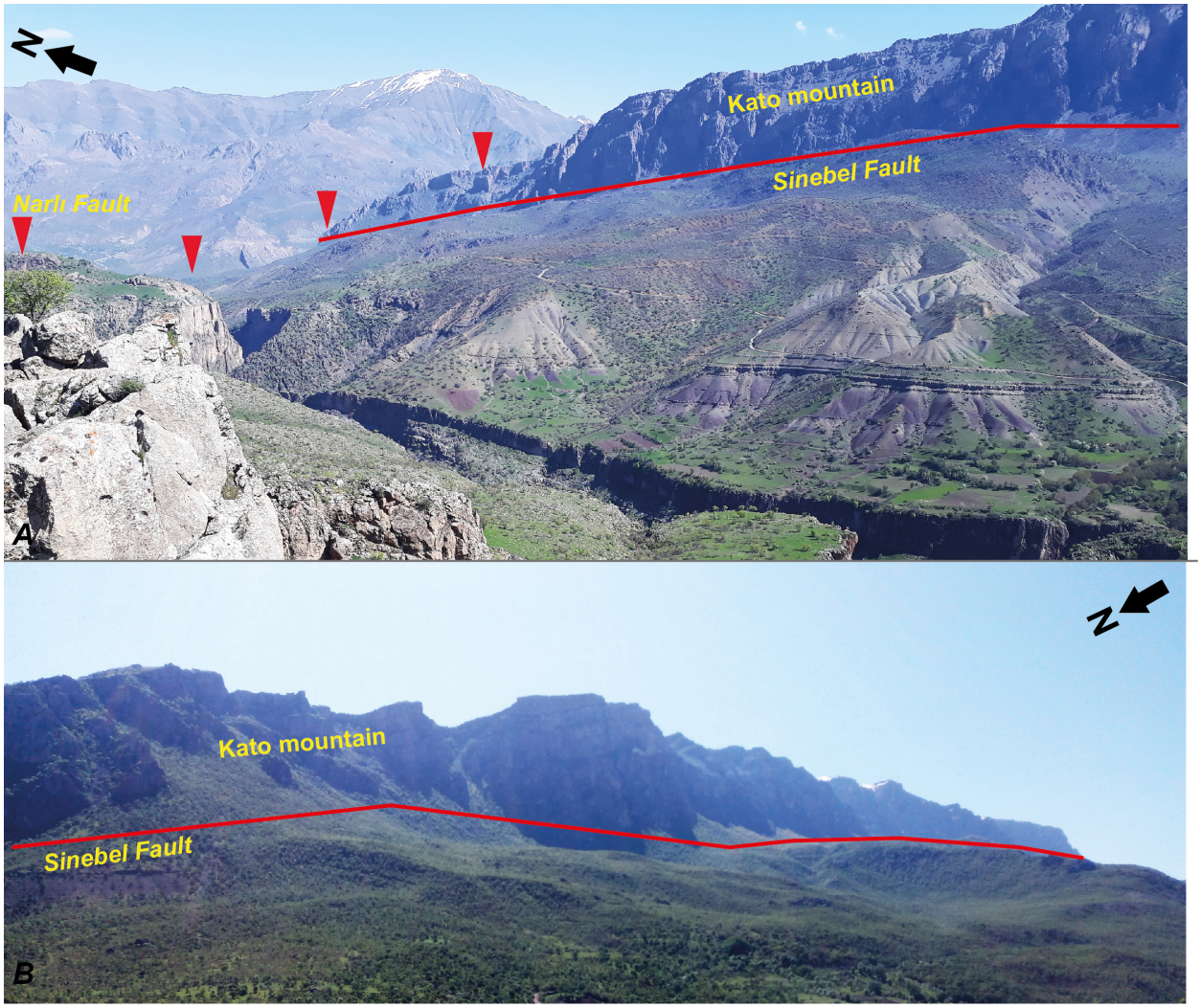


**Figure 13.** The fault morphology developed in front of the Sinebel Fault, A) the northern part, B) the southern part.

direction. The most important indicators of this extension are the NNW-SSE trending normal faults developed on the western slope of Kato Mountain, with a hanging valley and karstification surface. In addition, the Sinebel River has a meandering form and expressed high erosion rates during tectonic uplift, confirming the Sinebel Valley is an antecedent valley.

(iii) The high erosion rate in parallel with the development of the main structures controlling the topography of the region shows the effects of the compression on the terrain. Furthermore, the rough topography of the areas where there are pure thrust faults is not present in the transfer zone. The deformation rate is especially high in the hanging wall blocks and is lower in the footwall blocks.

(iv) Relative uplift rates vary across the region with rates higher than 0.4 mm year$^{-1}$ in the northwestern and southern parts of the study area. Although the lowest uplift rate measured was across the Sinebel Fault, the four terraces' levels observed in the Sinebel Valley show that this region was affected by multiple sudden uplift events. Because Sinebel Valley continues its development with the transfer zone that developed between Şirvan and Hakkâri Segments. Accordingly, the deformation rate increases from north to south in the valley morphology and the meander morphology is breaking down.

As a result, this study indicated that the temporal topographic evolution in such thrust belts is the result of tectonic structures with different characteristics, not just thrust faults.

**Acknowledgments**
We would like to thank the excellent reviews by Jamal A. H. Doski, anonymous reviewers and the editor Taylan Sançar which greatly improved the final manuscript.

## References


Agard P, Omrani J, Jolivet L, Whitechurch H, Vrielynck B et al. (2011). Zagros orogeny: a subduction-dominated process. Geological Magazine 148 (5-6): 692–725. https://doi.org/10.1017/S001675681100046X

Aktürk A (1985). Çatak-Narlı (Van) yöresinin stratigrafisi ve tektoniği. PhD, Fırat University, Elazığ, Turkey (in Turkish).

Al-Lazki AI, Sandvol E, Seber D, Barazangi M, Turkelli N et al. (2004). Pn tomographic imaging of mantle lid velocity and anisotropy at the junction of the Arabian, Eurasian and African Plates. Geophysical Journal International 158: 1024–1040. https://doi.org/10.1111/j.1365-246X.2004.02355.x

Allen M, Jackson JA, Walker R (2004). Late Cenozoic reorganization of the Arabia– Eurasia collision and the comparison of short-term and long-term deformation rates. Tectonics 23 (2): TC2008. https://doi.org/10.1029/2003TC001530

Allen MB, Kheirkhah M, Emami MH, Jones SJ (2011). Right-lateral shear across Iran and kinematic change in the Arabia–Eurasia collision zone. Geophysical Journal International 184 (2): 555-574. https://doi.org/10.1111/j.1365-246X.2010.04874.x

Allmendinger RW, Jordan TE, Kay SM, Isacks BL (1997). The evolution of the Altiplano-Puna plateau in the Central Andes. Annual Review of Earth and Planetary Sciences 25: 139–174. https://doi.org/10.1146/annurev.earth.25.1.139

Andreani L, Gloaguen R (2016). Geomorphic analysis of transient landscapes in the Sierra Madre de Chiapas and Maya Mountains (northern Central America): Implications for the North American-Caribbean-Cocos plate boundary. Earth Surface Dynamics 4: 71–102. https://doi.org/10.5194/esurf-4-71-2016

Azor A, Keller EA, Yeats RS (2002). Geomorphic indicators of actiand fold growth: South Mountain-Oak Ridge anticline, Andntura basin, southern California. Geological Society of America Bulletin 114 (6): 745-753. https://doi.org/10.1130/0016760 6(2002)114%3C0745:GIOAFG%3E2.0.CO;2

Bahrami S (2013). Tectonic controls on the morphometry of alluvial fans around Danehkhoshk anticline, Zagros, Iran. Geomorphology 180–181: 217–230. https://doi.org/10.1016/j.geomorph.2012.10.012

Bakkal B, Çinku MC, Heller F (2019). Paleomagnetic results along the Bitlis-Zagros suture zone in SE Anatolia, Turkey: Implications for the activation of the Dead Sea Fault Zone. Journal of Asian Earth Sciences 172: 14-29. https://doi.org/10.1016/j.jseaes.2018.08.026

Barka AA, Reilinger R (1997). Active tectonics of the Eastern Mediterranean region: deduced from GPS, neotectonic and seismicity data. Annali di Geofisica 40 (3): 587-610. https://doi.org/10.4401/ag-3892

Baulig H (1926). Sur une méthode d'analyse altimétrique appliquée à la Bretagne. Bulletin de l'Association de Géographes Français 10: 7–9.

Berberian M (1995). Master "blind" thrust faults hidden under the Zagros folds: active basement tectonics and surface morphotectonics. Tectonophysics 241: 193–224. https://doi.org/10.1016/0040-1951(94)00185-C

Bishop P (2007). Long-term landscape evolution: linking tectonics and surface processes. Earth Surface Processes and Landforms 32: 329–365. https://doi.org/10.1002/esp.1493

Blanc EJP, Allen MB, Inger S, Hassani H (2003). Structural styles in the Zagros Simple Folded Zone, Iran. Journal of the Geological Society 160: 401–412. https://doi.org/10.1144/0016-764902-110

Blanckenburg VF (2005). The control mechanisms of erosion and weathering at basin scale from cosmogenic nuclides in river sediment. Earth and Planetary Science Letters 237: 462– 479. https://doi.org/10.1016/j.epsl.2005.06.030

Bretis B, Bartl N, Grasemann B (2011). Lateral fold growth and linkage in the Zagros fold and thrust belt (Kurdistan, NE Iraq). Basin Research 23: 615–630. https://doi.org/10.1111/j.1365-2117.2011.00506.x

Bull WB (1977). Tectonic Geomorphology of the Mojave Desert, California, US, Geological Survey Contract Report 14-08-001-G-394, Office of Earthquakes, Volcanoes, and Engineering, pp.188.

Bull WB, McFadden LD (1977). Tectonic geomorphology north and south of the Garlock fault, California, Proceedings of the 8th Annual Geomorphology Symposium, Doehring, D.O., (Ed), State University of New York, Binghamton, 115–138.

Burbank DW, Anderson RS (2012). Tectonic Geomorphology, second ed. Wiley-Blackwell.

Copley A, Jackson J (2006). Active tectonics of the Turkish-Iranian Plateau. Tectonics 25: TC6006. https://doi.org/10.1029/2005TC001906

Csontos L, Sasvári Á, Pocsai T, Kósa L, Salae AT et al. (2012). Structural evolution of the northwestern Zagros, Kurdistan Region, Iraq: Implications on oil migration. GeoArabia 17 (2): 81–116. https://doi.org/10.2113/geoarabia170281

Cyr DE, Granger AJ, Olivetti V, Molin P (2010). Quantifying rock uplift rates using channel steepness and cosmogenic nuclide-determined erosion rates: examples from northern and southern Italy. Lithosphere 2: 188-198. https://doi.org/10.1130/L96.1

Dahlstrom CDA (1970). Structural geology in the eastern margin of the Canadian Rocky Mountains. Bulletin of Canadian Petroleum Geology 18 (3): 332–406. https://doi.org/10.35767/gscpgbull.18.3.332

Davis WM (1902). Base-level, grade, and peneplain, The Journal of Geology 10 (1): 77-111.

De Righi MR, Cortesini A (1964). Gravity tectonics in foothills structure belt of southeast Turkey. American Association of Petroleum Geologists 48 (12): 1911-1937. https://doi.org/10.1306/A66334D8-16C0-11D7-8645000102C1865D

Delcaillau B, Carozza JM, Laville E (2006). Recent fold growth and drainage development: The Janauri and Chandigarh anticlines in the Siwalik foothills, northwest India. Geomorphology 76: 241-256. https://doi.org/10.1016/j.geomorph.2005.11.005

Dercourt J, Zonenshain LP, Ricou LE, Kazmin VG, Lepichon X et al. (1986). Geological evolution of the Tethys belt from the Atlantic to the Pamirs since the Lias. Tectonophysics 123 (1–4): 241–315. https://doi.org/10.1016/0040-1951(86)90199-X

Dewey JF, Pitman WC, Ryan WBF, Bonnin J (1973). Plate tectonics and evolution of alpine system. Geological Society of American Bulletin 84 (10): 3137–3180. https://doi.org/10.1130/0016-7606(1973)84b3137:ptateo>2.0.co;2

Dewey JF, Hempton MR, Kidd WSF, Şaroğlu F, Şengör AMC (1986). Shortening of continental lithosphere: the neotectonics of Eastern Anatolia a young collision zone, in: Coward, M.P., Ries, A.C. (Eds.), Collision Tectonics. Geological Society, London, Special Publications: 19: 1-36 (Robert M. Shackleton volume). https://doi.org/10.1144/GSL.SP.1986.019.01.01

DiBiase R, Whipple KX, Heimsath AM, Ouimet WB (2010). Landscape form and millennial erosion rates in the San Gabriel Mountains. Earth and Planetary Science Letters 289: 134-144. https://doi.org/10.1016/j.epsl.2009.10.036

Doğan U (2005). Land subsidence and caprock dolines caused by subsurface gypsum dissolution and the effect of subsidence on the fluvial system in the Upper Tigris Basin (Between Bismil–Batman, Turkey). Geomorphology, 71: 389-401. https://doi.org/10.1016/j.geomorph.2005.04.010

Doğan U, Koçyiğit A, Gökkaya E (2017). Development of the Kembos and Eynif structural poljes: Morphotectonic evolution of the Upper Manavgat River basin, central Taurides, Turkey. Geomorphology 278: 105-120. https://doi.org/10.1016/j.geomorph.2016.10.030

Doski JAH, McClay K (2022) Tectono-stratigraphic evolution, regional structure and fracture patterns of the Zagros fold-thrust belt in the Duhok region, Kurdistan, northern Iraq. Tectonophysics 838: 229506. https://doi.org/10.1016/j.tecto.2022.229506

Duman TY, Robertson AH, Elmacı H, Kara M (2017). Palaeozoic-Recent geological development and uplift of the Amanos Mountains (S Turkey) in the critically located northwestern most corner of the Arabian continent. Geodinamica Acta 29 (1): 103-138. https://doi.org/10.1080/09853111.2017.1323428

Emre Ö, Duman TY, Özalp S, Elmacı H, Olgun Ş et al. (2013). Active Fault Map of Turkey with an Explanatory Text. 1:1,250,000 Scale, General Directorate of Mineral Research and Exploration, Ankara.

Erol O (2001). Geomorphological evolution of some karstic terrains in the Southwestern Turkey. Present state and future trends of Karst studies. Proceeding of the 6th International Symposium and Field Seminar, Turkey, pp. 473-484.

Faulds JE, Varga RJ (1998). The role of accommodation zones and transfer zones in the regional segmentation of extended terranes. Geological Society of America Special Paper 323, https://doi.org/10.1130/0-8137-2323-X.1

Font M, Amorese D, Lagarde JL (2010). DEM and GIS analysis of the stream gradient index to evaluate effects of tectonics: The Normandy intraplate area (NW France). Geomorphology 119: 172-180. https://doi.org/10.1016/j.geomorph.2010.03.017

Giaconia F, Rea GB, Martínez-Martínez JM, Azañón JM, Pérez-Peña JV et al. (2012). Geomorphic evidence of active tectonics in the Sierra Alhamilla (eastern Betics, SE Spain). Geomorphology 145–146: 90-106. https://doi.org/10.1016/j.geomorph.2011.12.043

Giamboni M, Wetzel A, Schneider B (2005). Geomorphic response of alluvial rivers to active tectonics: Example from the southern Rhine graben. Austrian Journal of Earth Sciences. 97: 24– 37.

Gordon JE, Thompson DBA, Haynes VM, McDonald R, Brazier V (1998). Environmental sensitivity and conservation management in the Cairngorm Mountains, Scotland. Ambio 27 (4): 335–344.

Granger DE, Riebe CS (2007). Cosmogenic nuclides in weathering and erosion. In: Holland HD, Turekian KK (eds) Surface and ground water, weathering, and soils. Treatise on Geochemistry 5:1–43. https://doi.org/10.1016/B978-0-08-095975-7.00514-3

Grohmann CH (2004). Morphometric analysis in geographic information systems: Applications of free software GRASS and R. Computers & Geosciences 30 (9-10): 1055-1067. https://doi.org/10.1016/j.cageo.2004.08.002

Hall R (1976). Ophiolite emplacement and the evolution of the Taurus suture zone, southeastern Turkey. Geological Society of America Bulletin 87 (7): 1078-1088. https://doi.org/10.1130/0016-7606(1976)87<1078:OEATEO>2.0.CO;2

Harzhauser M, Kroh A, Mandic O, Piller EW, Gohlich U et al. (2007). Biogeographic responses to geodynamics: a key study all around the Oligo-Miocene Tethyan Seaway. Zoologischer Anzeiger- A Journal of Comparative Zoology 246 (4): 241–256. https://doi.org/10.1016/j.jcz.2007.05.001

Hempton MR (1984). Result of detailed mapping near lake Hazar (eastern Taurus Mountains), in: Tekeli, O., Göncüoğlu, M.C. (Eds.), Geology of the Taurus Belt. Int Symp Proc of Bulletin of the Mineral Research and Exploration, Ankara, pp. 223–228.

Hempton MR (1985). Structure and deformation history of the Bitlis suture near Lake Hazar, Southeastern Turkey. Geological Society of America Bulletin 96 (2): 233–243. https://doi.org/10.1130/0016-7606

Hempton MR (1987). Constraints on Arabian plate motion and extensional history of the Red Sea. Tectonics 6 (6): 687-705. https://doi.org/10.1029/TC006i006p00687

Hergarten S, Robl J, Stüwe K (2014). Extracting topographic swath profiles across curved geomorphic features. Earth Surface Dynamics 2 (1): 97-104. https://doi.org/10.5194/esurf-2-97-2014, 2014

Hessami K, Pantosti D, Tabassi H, Shabanian E, Abbassi M et al. (2003). Paleoearthquakes and slip rates of the North Tabriz Fault, NW Iran: preliminary results. Annals of Geophysics 46 (5): 903–915. https://doi.org/10.4401/ag-3461

Hessami K, Nilforoushan F, Talbot CJ (2006). Active deformation within the Zagros Mountains deduced from GPS measurements. Journal of the Geological Society 163: 143-148. https://doi.org/10.1144/0016-764905-031

Hobson RD (1972). Surface roughness in topography: quantitative approach, in Chorley R, Methuen J (Eds.), Spatial analysis in geomorphology, London, 225–245.

Homke S, Vergés J, Garcés M, Emami H, Karpuz R (2004). Magnetostratigraphy of Miocene-Pliocene Zagros foreland deposits in the front of the Push-e Kush Arc (Lurestan Province, Iran). Earth and Planetary Science Letters 225 (3-4): 397–410. https://doi.org/10.1016/j.epsl.2004.07.002

Jackson JA, Van Dissen R, Berryman K (1998). Tilting of active folds and faults in the Manawatu region, New Zealand: evidence from surface drainage patterns, New Zealand Journal of Geology and Geophysics 41 (4): 377–385. https://doi.org/10.1080/00288306.1998.9514817

Jassim SZ, Goff JC (2006). Geology of Iraq, first ed., Published by Dolin, Prague and Moravian Museum, Brno, Printed in the Czech Republic.

Karakhanian AS, Trifonov VG, Philip H, Avagyan A, Hessami K et al. (2004). Active faulting and natural hazards in Armenia, eastern Turkey and northwestern Iran. Tectonophysics 380 (3-4): 189-219. https://doi.org/10.1016/j.tecto.2003.09.025

Keller EA (1986). Investigation of Active Tectonics: Use of Surficial Earth Processes, in: Active Tectonics, Studies in Geophysics, Chapter 8, National Academy Press, Washington DC, pp.136-147.

Keller EA, Pinter N (2002). Active Tectonics. Second ed. Prentice Hall, Upper Saddle Rivers, pp. 363.

Keller EA, Seaver DB, Laduzinsky DL, Johnson DL, Ku TL (2000). Tectonic geomorphology of active folding over buried reverse faults: San Emigdio Mountain front, southern San Joaquin Valley, California, Geology Society America Bulletin 112 (1): 86–97. https://doi.org/10.1130/0016-7606(2000)112.

Kelling G, Gökçen SL, Floyd PA, Gökçen N (1987). Neogene tectonics and plate convergence in the eastern Mediterranean: New data from southern Turkey. Geology 15 (5): 425–429. https://doi.org/10.1130/0091-7613(1987)15<425:NTAPCI>2.0.CO;2

Ketin İ (1966). Cambrian outcrops in southeastern Turkey and their comparison wıth the Cambrian of East Iran. Bulletin of The Mineral Research and Exploration 66: 75-87.

King G, Yielding G 1984. The evolution of a thrust fault system: processes of rupture initiation, propagation and termination in the 1980 El Asnam (Algeria) earthquake. Geophysical Journal of the Royal Astronomical Society 77 (3): 915-933. https://doi.org/10.1111/j.1365-246X.1984.tb02229.x

Kirby E, Whipple K (2001). Quantifying differential rock-uplift rates via stream profile analysis. Geology 29 (5): 415-418. https://doi.org/10.1130/0091-7613.

Kirby E, Whipple K (2012). Expression of active tectonics in erosional landscapes. Journal of Structural Geology 44: 54-75. https://doi.org/10.1016/j.jsg.2012.07.009

Koçyiğit A, Yılmaz A, Adamia S, Kuloshvili S (2001). Neotectonics of East Anatolian Plateau (Turkey) and Lesser Caucasus: implication for transition from thrusting to strike-slip faulting. Geodinamica Acta 14 (1-3): 177–195. https://doi.org/10.1016/S0985-3111(00)01064-0

Koshnaw RI, Horton BK, Stockli DF, Barber DE, Tamar-Agha MY et al. (2017). Neogene shortening and exhumation of the Zagros fold-thrust belt and foreland basin in the Kurdistan region of northern Iraq. Tectonophysics 694: 332–355. https://doi.org/10.1016/j.tecto.2016.11.016

Marr JC, Swenson JB, Paola C, Voller VR (2000). A two-diffusion model of fluvial stratigraphy in closed depositional basins. Basin Research 12 (3-4): 381-398. https://doi.org/10.1046/j.1365-2117.2000.00134.x

McClusky S, Balassanian S, Barka A, Demir C, Ergintav S et al. (2000). Global Positioning System constraints on plate kinematics and dynamics in the eastern Mediterranean and Caucasus. Journal of Geophysical Research Atmospheres 105 (B3): 5695-5719. https://doi.org/10.1029/1999JB900351

McClusky SM, Reillinger R, Mahmoud S, Ben Sari D, Tealeb A (2003). GPS constraints on Africa (Nubia) and Arabia plate motions. Geophysical Journal International 155 (1): 126–138. https://doi.org/10.1046/j.1365-246X.2003.02023.x

McQuarrie N (2004). Crustal scale geometry of the Zagros fold-thrust belt, Iran. Journal of Structural Geology 26 (3): 519–535. https://doi.org/10.1016/j.jsg.2003.08.009

McQuarrie N, Stock JM, Verdel C, Wernicke BP (2003). Cenozoic evolution of Neotethys and implications for the causes of plate motions. Goephysical Research Letters 30(20): 1-6. https://doi.org/10.1029/2003GL017992

Molinaro M, Leturmy P, Guezou JC, Frizon de Lamotte D, Eshraghi SA (2005a). The structure and kinematics of the south-eastern Zagros fold-thrust belt; Iran: from thin-skinned to thick-skinned tectonics. Tectonics 24: 1-19. https://doi.org/10.1029/2004TC001633

Molinaro M, Zeyen H, Laurencin X (2005b). Lithospheric structure underneath the SE Zagros Mountains, Iran: recent slab break-off? Terra Nova 17 (1): 1–6. https://doi.org/10.1111/j.1365-3121.2004.00575.x

Monod O, Kuzucuoğlu C, Okay A (2006). A Miocene palaeovalley network in the Western Taurus (Turkey). Turkish Journal of Earth Sciences 15 (1): 1-23.

Montgomery DR, Abbe TB, Buffington JM, Peterson NP, Schmidt KM et al. (1996). Distribution of bedrock and alluvial channels in forested mountain drainage basins. Nature 381: 587-589.

Mouthereau F, Lacombe O, Vergés J (2012). Building the Zagros collisional orogen: Timing, strain distribution and the Dynamics of Arabia/Eurasia plate convergence. Tectonophysics 532–535: 27–60. https://doi.org/10.1016/j.tecto.2012.01.022

Mouthereau F, Tensi J, Bellahsen N, Lacombe O, De Boisgrollier T et al. (2007). Tertiary sequence of deformation in a thin-skinned/thick-skinned collision belt: The Zagros Folded Belt (Fars, Iran). Tectonics 26: TC5006. https://doi.org/10.1029/2007TC002098

Nicoll K (2010). Landscape development within a young collision zone: implications for post-Tethyan evolution of the Upper Tigris River system in southeastern Turkey. International Geolology Review 52 (4-6): 404-422. https://doi.org/10.1080/00206810902951072

Okay A, Zattin M, Cavazza W (2010). Apatite fission-track data for the Miocene Arabia-Eurasia collision. Geology 38 (1): 35-38. https://doi.org/10.1130/G30234.1

Oral MB, Reilinger RE, Toksoz MN, King RW, Barka AA et al. (1995). Global positioning system offers evidence of plate motions in eastern Mediterranean. EOS, Transactions, American Geophysical Union 76 (2): 9–11. https://doi.org/10.1029/EO076i002p00009-01

Ouimet WB, Whipple KX, Granger DE (2009). Beyond threshold hillslopes: channel adjustment to base-level fall in tectonically active mountain ranges. Geology 37 (7): 579–582. https://doi.org/10.1130/G30013A.1

Öztürk Y, Zorer H (2020). Tectono-geomorphological shapes in Sinebel Gorge Valley and surrounding (Pervari/Siirt). International Journal of Geography and Geography Education 41: 367-395. https://doi.org/10.32003/igge.653711

Pérez-Peña JV, Azañón JM, Azor A (2009a). CalHypso: An ArcGIS extension to calculate hypsometric curands and their statistical moments. Applications to drainage basin analysis in SE Spain. Computers & Geosciences 35 (6): 1214-1223. https://doi.org/10.1016/j.cageo.2008.06.006

Pérez-Peña JV, Azañón JM, Booth-Rea G, Azor A, Delgado J (2009b). Differentiating geology and tectonics using a spatial autocorrelation technique for the hypsometric integral. Journal of Geophysical Research 114 (F2), F02018. https://doi.org/10.1029/2008JF001092

Pérez-Peña JV, Azañón JM, Azor A, Booth-Rea G, Galve JP et al. (2015). Quaternary landscape evolution driven by slab-pull mechanisms in the Granada Basin (Central Betics). Tectonophysics 663: 5–18. https://doi.org/10.1016/j.geomorph.2008.10.018

Perinçek D (1990). Stratigraphy of the Hakkâri province southeast Turkey. Bulletin of TAPG 2(1): 21-68 (in Turkish).

Perinçek D, Özkaya I (1981). Arabistan levhası kuzey kenarının tektonik evrimi. Earth Science 7 (8): 91-102 (in Turkish).

Philip H, Avagyan A, Karakhanian A, Ritz JF, Rebai S (2001). Estimating slip rates and recurrence intervals for strong earthquakes along an intracontinental fault: example of the Pambak–Sevan–Sunik fault (Armenia). Tectonophysics 343 (3–4): 205-232. https://doi.org/10.1016/S0040-1951(01)00258-X

Ramsey LA, Walker RT, Jackson J (2008). Fold evolution and drainage development in the Zagros mountains of Fars province, SE Iran. Basin Researchs 20 (1): 23– 48. https://doi.org/10.1111/j.1365-2117.2007.00342.x

Reilinger RE, McClusky S, Oral MB, King W, Toksoz MN (1997). Global positioning, system measurements of present-day crustal movements in the Arabian–Africa–Eurasia plate collision zone. Journal of Geophyical Research 102 (B5): 9983–9999. https://doi.org/10.1029/96JB03736

Reilinger R, McClusky S, Vernant P, Lawrence S, Ergintav S et al. (2006). GPS constraints on continental deformation in the Africa–Arabia, Eurasia continental collision zone and implications for the dynamics of plate interactions. Journal of Geophysical Research-Solid Earth 111: (B05411) https://doi.org/10.1029/2005JB004051

Rick Allmandinger's Stuff: https://rickallmendinger.net.

Robertson AHF (2000). Mesozoic-Tertiary tectonic-sedimentary evolution of a South Tethyan Oceanic Basin and its margins in Southern Turkey. Geological Society London Special Publications 173 (1): 97-138. https://doi.org/10.1144/GSL.SP.2000.173.01.05

Robertson AHF, Clift PD, Degnan PJ, Jones G (1991). Palaeogeographic and palaeotectonic evolution of the Eastern Mediterranean Neotethys. Palaeogeography, Palaeoclimatology, Palaeoecology 87 (1–4): 289-343. https://doi.org/10.1016/0031-0182(91)90140-M

Safran EB, Bierman PR, Aalto R, Dunne T, Whipple KX et al. (2005). Erosion rates driven by channel network incision in the Bolivian Andes. Earth Surface Processes and Landforms 30 (8): 1007-1024. https://doi.org/10.1002/esp.1259

Sağlam Selçuk A (2016). Evaluation of the relative tectonic activity in the eastern Lake Van basin, East Turkey. Geomorphology 270: 9-21. https://doi.org/10.1016/j.geomorph.2016.07.009

Sançar T (2021). Morphometric investigations on the NW Bitlis-Zagros Mountain range (SE Turkey): Implications for the internal deformation of the western Turkish-Iranian Plateau. Journal of Asian Earth Sciences 216: 104751. https://doi.org/10.1016/j.jseaes.2021.104751

Schumm SA (1993). River response to baselevel change: implications for sequence stratigraphy. The Journal of Geology 101 (2): 279–294.

Seyitoğlu G, Esat K, Kaypak B, Toori M, Aktuğ B (2019). Internal deformation of Turkish–Iranian plateau in the Hinterland of Bitlis–Zagros Suture Zone. In: Developments in Structural Geology and Tectonics (Vol. 3, pp. 161-244). Elsevier.

Shahzad F, Gloaguen R (2011). Tecdem: A MATLAB Based Toolbox For Tectonic Geomorphology, Part 1: Drainage Network Preprocessing And Stream Profile Analysis. Computers & Geosciences 37 (2): 250–260. https://doi.org/10.1016/j.cageo.2010.06.008

Siddiqui S, Castaldini D, Soldati M (2017). DEM-based drainage network analysis using steepness and Hack SL indices to identify areas of differential uplift in Emilia–Romagna Apennines, northern Italy. Arabian Journal of Geosciences 10 (3). https://doi.org/10.1007/s12517-016-2795-x

Sissakian VK (1997). Geological Map of Arbeel and Mahabad Quadrangles Sheets NJ-38- 14 and NJ-38-15, Scale 1:250.000.

Snyder NP, Whipple KX, Tucker GE, Merritts DJ (2000). Landscape response to tectonic forcing: Digital elevation model analysis of stream profiles in the Mendocino triple junction region, northern California. Geology Society American Bulletin 112 (8): 1250-1263. https://doi.org/10.1130\0016-7606

Strahler AN (1952). Hypsometric (area-altitude curve) Analysis of Erosional Topography. Geology Society American Bulletin 63: 1117-1141. https://doi.org/10.1130/0016-7606

Strahler A (1957). Quantitative Analysis of Watershed Geomorphology. Transactions, American Geophysical Union 38: 913-920. https://doi.org/10.1029/TR038i006p00913

Stampfli GM, Borel GD (2002). A plate tectonic model for the Paleozoic and Mesozoic constrained by dynamic plate boundaries and restored synthetic oceanic isochrones. Earth and Planatery Science Letters 196 (1–2): 17–33. https://doi.org/10.1016/S0012-821X(01)00588-X

Strak V, Dominguez S, Petit C, Meyer B, Loget N (2011). Interaction between normal fault slip and erosion on relief evolution: Insights from experimental modelling. Tectonophysics 513 (1-4): 1-19. https://doi.org/10.1016/j.tecto.2011.10.005

Stolar D, Roe G, Willett S (2007). Controls on the patterns of topography and erosion rate in a critical orogen. Journal of Geophysical Research 112 (F4). https://doi.org/10.1029/2006JF000713

Sung QC, Chen YC (2004). Self-affinity dimensions of topography and its implications in morphotectonics: an example from Taiwan. Geomorphology 62 (3–4): 181-198. https://doi.org/10.1016/j.geomorph.2004.02.012

Şaroğlu F, Emre Ö, Boray A (1987). Türkiye'nin diri fayları ve depremsellikleri. MTA. Report No: 5216.

Şaroğlu F, Güner Y (1981). Doğu Anadolu'nun jeomorfolojik gelişimine etki eden öğeler: Jeomorfoloji, tektonik, volkanizma ilişkileri. Bulletin of TJK 24: 39-50, (in Turkish with an abstract in English).

Şengör AMC (1979). Mid-Mesozoic closure of Permo–Triassic Tethys and its implications, Nature 279: 590–593.

Şengör AMC (2005). Repeated Independent Discovery and 'Objective Evidence'in Science: An Example from Geology. In Turkish Studies in the History and Philosophy of Science (pp. 113-135). Springer, Dordrecht.

Şengör AMC, Kidd WSF (1979). Postcollisional Tectonics of the Turkish Iranian Plateau and a Comparison with Tibet. Tectonophysics 55: 361-376.

Şengör AMC, Yılmaz Y (1981). Tethyan evolution of Turkey: A plate tectonic approach. Tectonophysics 75 (3-4): 181-190.

Şengör AMC, Görür N (1985) Strike-slip faulting and related basin formation in zones of tectonic escape: Turkey as a case study. In: Biddle K. and Christie-Blick N., Eds., Strike-Slip Deformation, Basin Formation and Sedimentation, Special Publications, SEPM Society for Sedimentary Geology, Tulsa, 37: 227-264.

Şengör AMC, Natal'in BA (2004). Phanerozoic analogues of Archaean oceanic basement fragments: Altaid ophiolites and ophirags. Developments in Precambrian Geology. 13: 675-726. https://doi.org/10.1016/S0166-2635(04)13021-1

Şengör AMC, Yılmaz Y, Özeren S, Zor E, Genç T (2003). Doğu Anadolu litosfer mekaniğine yeni bir yaklaşım. İTÜ Avrasya Yer Bilimi Enstitüsü. Kuvaterner Çalıştayı IV, 101- 110 (in Turkish).

Talebian M, Jackson J (2002). Offset on the main recent fault of NW Iran and implication for the Late Cenozoic tectonics of the Arabia-Eurasia collision zone. Geophysical Journal International 150 (2): 422-439. https://doi.org/10.1046/j.1365-246X.2002.01711.x

Tarolli P (2014). High-resolution topography for understanding Earth surface processes: Opportunities and challenges. Geomorphology 216: 295–312. https://doi.org/10.1016/j.geomorph.2014.03.008

Telbisz T, Kovács G, Székely B, Szabó J (2013). Topographic swath profile analysis: a generalization and sensitivity evaluation of a digital terrain analysis tool. Zeitschrift für Geomorphologie 57 (4): 485-513. https://doi.org/10.1127/0372-8854/2013/0110

Usta SG (2015). Morphometric analysis of active tectonic imprints at the junction of Büyük Menderes and Bozdoğan grabens, Western Anatolia. PhD, Middle East Technical University, Ankara, Turkey (in Turkish).

Vanlaningham S, Meigs A, Goldfinger C (2006). The effects of rock uplift and rock resistance on river morphology in a subduction zone forearc, Oregon, USA. Earth Surface Processes and Landforms 31 (10): 1257-1279. https://doi.org/10.1002/esp.1326

Vergés J, Saura E, Casciello E, Fernàndez M, Villaseñor A et al. (2011). Crustal-scale cross-sections across the NW Zagros belt: Implications for the Arabian margin reconstruction. Geological Magazine 148 (5-6): 739–761. https://doi.org/10.1017/S001675681100033

Vernant P, Nilforoushan F, Hatzfeld D, Abbassi M, Vigny C et al. (2004). Contemporary crustal deformation and plate kinematics in middle east constrained by GPS measurements in Iran and Northern Oman. Geophysical Journal International 157 (1): 381-398. https://doi.org/10.1111/j.1365-246X.2004.02222.x

Whipple KX (2004). Bedrock rivers and the geomorphology of active orogens. Annual Review of Earth and Planetary Sciences 32: 151-185. https://doi.org/10.1146\annurev.earth-.32.101802.120356

Whipple KX (2009). The influence of climate on the tectonic evolution of mountain belts. Nature Geoscience 2 (2): 97–104. https://doi.org/10.1038/ngeo413

Whipple KX, Tucker GE (1999). Dynamics of the stream-power river incision model: Implications for height limits of mountain ranges, landscape response timescales, and research needs. Journal of Geophysical Research 104 (B8): 17661–17674. https://doi.org/10.1029/1999JB900120

Whittaker AC (2012). How do landscapes record tectonics and climate? Lithosphere 4 (2): 160–164. https://doi.org/10.1130/RF.L003.1

Willett SD (1999). Orogeny and orography: The effects of erosion on the structure of mountain belts. Journal of Geophysical Research 104 (B12): 28,957–28,981. https://doi.org/10.1029/1999JB900248

Wilson JT (1966). Did the Atlantic close and then re-open? Nature 211: 676–681. https://doi.org/10.1038/211676a0

Wobus C, Whipple KX, Kirby E, Snyder N, Johnson J et al. (2006). Tectonics from topography: procedures, promise, and pitfalls. In: Sean D Willett, Niels Hovius, Mark T Brandon, Donald M Fisher (Eds.) Tectonics, Climate, and Landscape Evolution. Geological Society of America. 398: 55–74. https://doi.org/10.1130/2006.2398(04)

Yılmaz Y (1993). New evidence and model on the evolution of the southeast Anatolian orogen. Geology Society American Bulletin 105 (2): 251-271. https://doi.org/10.1130/0016-7606(1993)105<0251:NEAMOT>2.3.CO;2

Yiğitbaş E, Yılmaz Y (1996). New evidence and solution to the Maden complex controversy of the Southeast Anatolian orogenic belt (Turkey). Geologische Rundschau 85: 250–263. https://doi.org/10.1007/BF02422232

Zebari M, Burberry CM (2015). 4-D evolution of anticlines and implications for hydrocarbon exploration within the Zagros Fold-Thrust Belt, Kurdistan Region, Iraq. GeoArabia 20: 161–188. https://doi.org/10.2113/geoarabia2001161

Zebari M, Grützner C, Navabpour P, Ustaszewski K (2019). Relative timing of uplift along the Zagros Mountain Front Flexure (Kurdistan Region of Iraq): Constrained by geomorphic indices and landscape evolution modeling. Journal Geophysical Research Solid Earth 10: 663–682. https://doi.org/10.5194/se-10-663-2019

Zorer H, Öztürk Y (2021). Fluvio-karstic development of the Masiro Canyon (Pervari) and geomorphic features of its surroundings. Journal Geography 42: 49-65. http://doi.org/10.26650/jgeog2021-825470